学位論文（要約）

Revealing the biogeochemical cycles of the hypersaline environments based on the organic geochemical approaches

（有機地球化学的手法による高塩環境の生物地球化学循環の解明）

平成 29 年 12 月博士（理学）申請

東京大学大学院理学系研究科
地球惑星科学専攻

伊左治 雄太

Revealing the biogeochemical cycles of the hypersaline environments based on the organic geochemical approaches

by

Yuta ISAJI

Department of Earth and Planetary Science
Graduate School of Science
The University of Tokyo

submitted to the University of Tokyo
In partial fulfillment of the requirements for the Degree of Doctor of Philosophy

December 20, 2017

Abstract

Hypersaline environments are among the most extreme environments on the Earth, imposing strong stresses on biological systems. The selection pressure results in a unique microbial community dominated by specific halophilic microorganisms, which should associate modifications in biogeochemical cycle. Importantly, a variety of hypersaline environments, in terms of physical and chemical properties, are formed in the modern Earth surface as well as in the past. Thus, the Earth surface system and inhabiting organisms have experienced a variety of hypersaline condition throughout the Earth's history. Despite such importance, our knowledge on the biogeochemistry of hypersaline environments is still fragmentary, and much less is known on its response during the past massive evaporation events.

The present work focused on the carbon and nitrogen cycles of two distinct hypersaline environments; the solar salterns as an example of the modern shallow hypersaline environment, and the massive evaporation event in the late Miocene, the Messinian Salinity Crisis (MSC). The solar salterns is characterized by formation of a highly productive microbial mat inhabited by diverse groups of microorganisms, which enables us to investigate the response of biological activities and biogeochemical cycle to increasing salinity. On the other hand, more than 1 million km^3 of salts were precipitated over the Mediterranean basin during the MSC between 5.97 and 5.33 Ma. Because there is no modern analogue of a comparable scale, investigation of this events should broaden our understanding of the biogeochemical cycle of hypersaline environments.

In the solar salterns, the biomass and primary productivity of the benthic microbial mats were substantially higher than that of the water column. The isotopic fractionation factor during uptake of carbon by phototrophs along the salinity gradient, calculated from

$\delta^{13}C$ of chlorophyll *a* and β-carotene, indicated that the primary production was suppressed as the salinity increased. Such modification of the biological activity resulted in large variation in $\delta^{13}C$ of dissolved inorganic carbon (DIC) in the brine. While active photosynthesis consuming CO_2(aq) in the carbonate and gypsum ponds (degree of evaporation: 2–10) induced dissolution of ^{13}C-depleted CO_2(gas) into the brine ($\delta^{13}C_{DIC}$ = −5.0‰–−10.6‰), its suppression in the subsequent ponds resulted in the dominance of degassing of ^{13}C-depleted CO_2(aq) from the brine ($\delta^{13}C_{DIC}$ = 7.2‰ in the halite pond).

By contrast, the depth profiles of $\delta^{15}N$ of nitrate, ammonium, and chloropigments in the microbial mats of the carbonate and gypsum ponds indicate that common processes control the nitrogen cycle in the hypersaline microbial mats across a wide salinity range. Ammonium accumulated in the anoxic layer of the mat as a result of anaerobic degradation of organic matter and suppression of nitrification, and was assimilated by purple sulfur bacteria and cyanobacteria as it diffused upwards through the mat. These processes efficiently recycled nitrogen within the mat, resulting in high primary productivity of this ecosystem. Another important finding was that $\delta^{15}N$ of the surface brine ammonium became enriched in ^{15}N due to degassing of ^{15}N-depleted dissolved ammonia induced by enhanced salinity ($\delta^{15}N_{NH4+}$ = 34.0‰ in the halite pond). It is thus concluded that ^{15}N-enriched ammonium is a specific characteristic of an actively evaporating environment and that ammonium plays an important role in the nitrogen cycles of the hypersaline environments.

During the first stage of MSC between 5.97 and 5.60 Ma, up to 16–17 cycles of gypsum–shale couplets deposited in the marginal sub-basins across the Mediterranean. I investigated the shale layers in the Vena del Gesso Basin (Northern Apennines, Italy). These layers were deposited under density-stratified condition formed due to the inflow of continental water over gypsum-precipitating brine during the humid climate phase of

~21 kyr precessional cycle. While similar shifts in the $\delta^{13}C$ values of total organic carbon and porphyrins derived from chlorophyll *c* suggest the predominance of eukaryotic algae, $\delta^{15}N$ of the porphyrins ranging from −6.5‰ to −5.4‰ indicate that phototrophs assimilated nitrogen supplied by diazotrophic cyanobacteria. These observations indicate that diazotrophic–diatom associations may have been of particular importance, considering their adaptation to stratified oligotrophic condition and rapid export production. Such condition probably resulted from conversion of ammonium into N_2 through nitrification–denitrification coupling near the pycnocline, inducing nitrogen-depletion in the surface photic zone. Active N_2-fixation at the surface balanced the loss of nitrogen by denitrification, establishing dynamic equilibrium of the biologically-available nitrogen like in the modern oceans.

Another example of freshwater–brine stratification is from the shale layers of the halite–shale couplets deposited annually during the peak of MSC (5.60–5.55 Ma) in the Caltanissetta Basin (Sicily, Italy). The geoporphyrins purified from this shale layer was extremely enriched in ^{15}N ($\delta^{15}N$ = 17.2‰), which is interpreted to reflect phototrophic assimilation of ^{15}N-enriched subsurface ammonium produced due to degassing of dissolved ammonia during the arid season. Such contrasting result compared to the freshwater–brine stratification during the first stage of MSC can be attributed to thin freshwater layer with shallow pycnocline under light-abundant condition, resulting in predominance of phototrophic assimilation of subsurface ammonium over nitrification–denitrification coupling. These results imply that evaporation–precipitation balance in the Mediterranean Sea during the MSC has the potential to shift the mode of the nitrogen cycle (nitrification–denitrification–N_2-fixation coupling vs. phototrophic assimilation of subsurface ammonium) through changing the depth of the chemocline.

Finally, based on the insights obtained in this work and in previous studies, I

constructed the framework of the evolution of the biogeochemical cycle throughout the MSC. It is speculated that the cyclical formation of different types of density stratification (i.e., thick freshwater–brine, thin freshwater–brine, brine–brine), which are produced in response to the climatic condition changing at various timescales, results in substantial shifts in the mode of carbon and nitrogen cycles. Such variation potentially has strong influence on the atmospheric CO_2 level and hence the global climate system.

Acknowledgements

I am deeply grateful to all the people who supported and advised me in completing my PhD research. I would like to deeply appreciate my supervisor, Dr. H. Kawahata, who has taught me what a scientist is and provided me the opportunity and the freedom to explore the vast frontiers of the Earth science. I would like to express my greatest appreciation to Dr. N. Ohkouchi for the considerable supports, discussions, and advices on all aspects of my research. Excitement of the science I learned from him is the driving force of my research. I would like to deeply appreciate Dr. J. Kuroda for introducing me the theme of my PhD research, and giving me constructive advices and warm encouragements throughout the years. He kindly introduced me many outstanding researchers for conducting various analyses, which broadened my field of the Earth science. I would like to express my deep gratitude to Dr. T. Yoshimura for his great supports in my research, and also for teaching me the basics of the inorganic geochemical analyses. Friendly and constructive discussions with him was always stimulating and fruitful. I greatly appreciate Dr. N. O. Ogawa for her technical advices on the organic geochemical analyses and teaching me her deep insights of the modern ecosystem. My research could not have been accomplished without the outstanding quality of her isotope measurements using the nano-EA/IRMS. Dr. Y. Takano is greatly appreciated for the technical advices on the HPLC and instructing me the operation of LC/MS. His deep knowledge on the organic geochemistry was also a great help in proceeding my research. I would like to express my deep gratitude to Ms. H. Suga, who kindly taught me the basics of the organic geochemical analyses. Her strictness in keeping the quality of the analysis is my role model. I am deeply grateful to Dr. F. J. Jiménez-Espejo for his constructive advices on my research. The sampling in Spain with his guidance was a valuable and exciting experience. I greatly thank Dr. S. Lugli for introduction on the Messinian Salinity

Crisis, helpful discussions, and enthusiastic supports during the sampling in Sicily. This research could not have been accomplished without the geological researches of his team.

I am greatly indebted to the following persons for their supports in my PhD research. I thank Dr. A. Makabe for the measurements of the concentrations and the nitrogen isotopic compositions of nitrate and ammonium in the brines. Dr. Y. Tamenori supported me on the X-ray fluorescence analysis of the evaporate rocks at Spring-8. Dr. A. Suzuki was helpful in the measurements of salinity and total alkalinity of the brines. Dr. T. Shibuya helped me to determine the concentration of the major ions in the brines. I thank Dr. A. Santulli for guiding me through the solar salterns in Trapani, Sicily, and providing me the basic information on the solar salterns ecosystem. Drs. F. J. Sierro and J. A. Flores are appreciated for guiding me during the sampling in Spain. Dr. K. Nagashima supported me on the X-ray diffraction analysis of the deposits in the solar salterns. Drs. V. Manzi, and M. Roveri are acknowledged for the insightful comments on the manuscripts. I also thank Dr. Dr. Y. Suzuki, D. Araoka, Dr. A. Ijiri, and Dr. T. Toyofuku for their discussions and helps in the analyses. Ms. A. Toki and K. Ishikawa helped me on the preparation of the samples before the analyses. I also deeply appreciate stimulating discussions and supports from the members in OFGS of Atmosphere and Ocean Research Institute) and the Department of Biogeochemistry of JAMSTEC.

Finally, I would like to express my greatest gratitude to my parents, sisters, and grandparents for their support of my life.

Contents

CHAPTER I

GENERAL INTRODUCTION

I-1. General Introduction

Hypersaline environments are among the most extreme environments on the Earth because physical and chemical parameters (osmotic pressure, water activity, chaotropic activity, *p*H, etc.) impose strong stresses on biological systems (e.g., Brown, 1990; Hallsworth et al., 2007). Strong selection pressure reduces both eukaryotic and prokaryotic diversity along the salinity gradient, resulting in a unique microbial community dominated by specific halophilic microorganisms (Oren, 1999; Benlloch et al., 2002; Ley et al., 2006). Importantly, biogeochemical cycle must also have been modified in response to the changes in physical and chemical properties of the solution and the biological activities.

Hypersaline environments are formed by several processes: (1) conversion of liquid water to gaseous phase through evaporation driven by the solar heat; (2) solidification of liquid water to ice under freezing temperature; (3) modification of the porewater chemistry in earth subsurface by diagenesis and metamorphism (Warren, 2016). A variety of hypersaline environments are formed in the modern Earth surface, each of which characterized by a unique ecosystem and biogeochemical cycle. Moreover, while the modern hypersaline environments are relatively small in scale, massive evaporation events are known to have occurred repeatedly in the geological past (Fig. I-1: Hay et al., 2006; Warren, 2010). Also, some studies suggest that the salinities of the Precambrian oceans were more than twice higher than the present (Knauth, 1998; Saito et al., 2016), implying that important evolutions of life (e.g., occurrence of stromatolites, emergence of oxygenic phototrophs) may have took place under hypersaline condition. Evaporites are also found in extraterrestrial materials, such as hydrated-salts on Mars (Ojha et al., 2015) and halite crystals trapping organic matter in the meteorites (Chan et al., 2018).

Thus, the Earth surface system and inhabiting organisms have experienced a variety

of hypersaline condition, in terms of scale, physical, and chemical properties of water, throughout the Earth's history (Fig. I-2). Despite such importance, our knowledge on the biogeochemistry of hypersaline environments is still fragmentary, in contrast to that of freshwater and marine settings, and much less is known on its response during the past massive evaporation events.

Elemental cycles of essential elements strongly influence microbial assemblages, and thus are critical components of biogeochemical cycle. In particular, nitrogen is a fundamental component of life playing an essential role in many biological processes, which makes nitrogen cycle a particularly important factor driving ecosystems. Organisms use energy to assimilate various nitrogenous compounds (e.g., NO_3^-, NH_4^+, N_2, organic nitrogen) to build their bodies, and also utilize them in dissimilatory processes (e.g., nitrification, denitrification, anammox) to obtain energy. The pool sizes of nitrogenous compounds and the flux to and from each pool are determined by the level of biological and physical processes (e.g., Brandes et al., 2007) which are strongly affected by environmental conditions, such as temperature, salinity, *p*H, redox conditions, and light availability. Extensive investigations have been conducted for the nitrogen cycles in freshwater and normal marine settings (e.g., Capone et al., 2008). Importantly, the modern marine nitrogen cycle is close to dynamic equilibrium, primarily due to tight coupling between N_2 fixation and denitrification (Brandes et al., 1998; Gruber, 2004; Deutsch et al., 2007; Ren et al., 2017).

The marine carbon cycle also plays a role in biogeochemical cycle, but more importantly, it is an essential component of the Earth's climate system because it controls the atmospheric CO_2 level (Shackleton, 2000; Zachos et al., 2001). Exchange of CO_2 between the atmosphere and oceans is primarily influenced by (1) the solubility of CO_2 which is a function of water temperature and salinity (the solubility pump: e.g., McGillis

and Wanninkhof, 2006), (2) the biological pump exporting organic matter fixed in the photic zone by primary production to the deep ocean (e.g., Berger et al., 1989; Kawahata et al., 2000; Honjo et al., 2008), and (3) the alkalinity pump absorbing CO_2 as a result of dissolution of calcium carbonates which increases alkalinity of the deep water (e.g., Boyle, 1988). Therefore, evaporation inducing changes in physical and chemical properties of water and biological activities has the potential to substantially modify the carbon cycle, and may strongly impact the climate system especially during the past massive evaporation events. Despite such importance, we only have limited insights into the carbon and nitrogen cycles of the modern hypersaline environments (e.g., Lazar and Erez, 1992; Canfield and Des Marais, 1993; Bebout et al., 1994; Isaji et al., 2017), and much less is known on their response during the massive evaporation events.

The natural abundances of stable carbon and nitrogen isotopes have been widely used to investigate biological and ecological processes. Because isotopic compositions of sources and products of biological processes are determined by isotopic fractionation associated with each biological processes, they provide process-related and source information which helps us elucidate the biogeochemical cycle of the system (Ohkouchi et al., 2015 and references therein). The discussions of the present work are mainly based on the stable carbon and nitrogen isotopic compositions ($\delta^{13}C$ and $\delta^{15}N$) of carbon and nitrogen substrates and organic molecules derived from specific source organisms (i.e., biomarkers). In particular, I used chloropigments (i.e., chlorophylls and bacteriochlorophylls), which are light-harvesting antenna pigments exclusively derived from phototrophs. The isotopic compositions of them record the physiology of phototrophs and substrates assimilated by them (Sachs and Repeta, 1999; Ohkouchi et al., 2005; York et al., 2007; Higgins et al., 2010; Isaji et al., 2015b; Naeher et al., 2016a, 2016b; Isaji et al., 2017). Significantly, degradation products of chloropigments,

geoporphyrins, are preserved in sediments on a geological timescale, making their isotopic compositions an ideal tool for obtaining information on the isotopic compositions of phototrophs and the biogeochemical cycles of past environments (Hayes et al., 1987; Boreham et al., 1989, 1990; Ocampo et al., 1989; Chicarelli et al., 1993; Keely et al., 1994; Ohkouchi et al., 2006; Kashiyama et al., 2008a, 2008b; Higgins et al., 2012; Junium et al., 2015).

In this dissertation, I focused on two distinct hypersaline environments; solar salterns as an example of the modern shallow hypersaline environment, and a massive evaporation event in the late Miocene, the Messinian Salinity Crisis (MSC). Solar salterns consist of a series of shallow ponds with salinity increasing from seawater up to the saturation point of halite (NaCl). A particular characteristic of these shallow hypersaline environments is the formation of a highly productive microbial mat inhabited by highly diverse groups of microorganisms (Ollivier et al., 1994; Oren, 2002; Ley et al., 2006). These characteristics enable us to investigate the responses of biological activities and biogeochemical cycle to increasing salinity.

The MSC is one of the most massive and dramatic evaporation event in Earth's history, precipitating more than 1 million km^3 of salts over the Mediterranean basin between 5.97 and 5.33 Ma (Hsü et al., 1973; Krijgsman et al., 1999; Rouchy and Caruso, 2006; Ryan, 2009; Roveri et al., 2014 and references therein). Because there is no modern analogue of a comparable scale, investigation of this events should broaden our understanding of the biogeochemical cycle in hypersaline environments. Moreover, because the MSC is the most recent massive evaporation event, such insights will also be the basis in extending our knowledge of the biogeochemistry of older evaporation events that occurred in a range of environmental settings.

This dissertation is composed of six chapters. In Chapters II and III, I aim to

understand the changes in chemical properties of evaporating brine and the responses of biological processes to increasing salinity in modern shallow hypersaline environment, the solar salterns. In Chapter II, salinity and major ion concentrations are measured to describe basic chemical properties of each pond in the solar salterns. Parameters related to carbonate system (concentration and $\delta^{13}C$ of dissolved inorganic carbon, total alkalinity, and *p*H) and carbon isotopic composition of pigments derived from phototrophs are measured to discuss the changes in carbonate system and primary productivity in response to increasing salinity. In Chapter III, I focuses on the nitrogen cycle of hypersaline environments. Discussions are based on the measurements of concentrations and $\delta^{15}N$ of nitrate and ammonium which enable us to trace processes occurring inside the microbial mats and surface brines. The nitrogen isotopic compositions of chloropigments provided information on the role of phototrophs in nitrogen cycle.

Chapters IV and V deal with the MSC. The objective of Chapter IV is to reveal the phototrophic community, carbon and nitrogen cycles, and depositional environment of the gypsum–shale couplets in the Northern Apennines of Italy and the Sorbas of Spain deposited during the initial stage of MSC between 5.97 and 5.60 Ma. This was achieved by determining the structures and measuring $\delta^{13}C$ and $\delta^{15}N$ of individual geoporphyrins extracted and purified from the deposits. In Chapter V, the peak of MSC between 5.60 and 5.55 Ma is investigated. Elemental mapping and chemical speciation using X-ray florescence technique, assignments of hydrocarbon biomarkers, and $\delta^{15}N$ measurements of geoporphyrins were conducted to elucidate the depositional environment and biological activity.

Finally, Chapter VI summarizes the conclusions of this dissertation. Based on the insights obtained in the present work, I also attempted to construct a comprehensive view of the evolution of biogeochemical cycle and its potential impact on the atmospheric CO_2

during the MSC.

I-2. Theoretical Backgrounds

There are two stable isotopes each in carbon and nitrogen, which have constant natural abundance ratio (^{12}C:^{13}C = 98.9:1.1 and ^{14}N:^{15}N = 99.6:0.4). This ratio in organisms differ from the natural abundance ratio, as a result of biological processes discriminating light and heavy isotopes. Because the variations in the isotopic compositions of natural sample materials are generally small, their ratios are expressed in the conventional δ notation relative to the isotopic composition of standard materials as follows:

$$\delta \equiv (R_{sample}/R_{standard} - 1) \times 10^3 \ (‰)$$

where R denotes the $^{13}C/^{12}C$ ratio for carbon and the $^{15}N/^{14}N$ ratio for nitrogen.

Discrimination of isotopes occurs during all physicochemical processes. The extent of discrimination is defined as isotopic fractionation (ε), which can be calculated from the isotopic compositions of the reactants (R_r) and products (R_p) as follows:

$$\varepsilon \equiv (R_r/R_p - 1) \times 10^3 \ (‰)$$

All physicochemical reactions can be classified into unidirectional (irreversible) and bidirectional (equilibrium) reactions, each of which described by different isotope effect. The isotope effect associated with bidirectional, equilibrium reaction is equilibrium isotope fractionation, where the isotopes are discriminated during the formation and destruction of the bonds involving the element of interest. For example, NH_3(aq) is reported to be depleted in ^{15}N by 45.4 ± 0.7‰ (± 1σ) relative to NH_4^+ in the following equilibrium reaction (Li et al., 2012):

$$NH_3(aq) + H_2O \rightleftarrows NH_4^+ + OH^-$$

The unidirectional reactions, on the other hand, are associated with kinetic isotopic fractionation, where the isotopes are discriminated as a result of the differences in

thermodynamic parameters and rate constants in chemical and biological reactions. The isotopic fractionation during such reactions approximately follows the Rayleigh distillation model, and the isotopic compositions of the reactant (δ_r) and products (δ_p) are conventionally described as follows:

$$\delta_r = \delta_0 - \varepsilon \ln f$$

$$\delta_p = \delta_0 + f / (1-f)\, \varepsilon \ln f$$

where δ_0 is the isotopic composition of reactant before the reaction, and f ($0 \leq f \leq 1$) is the fraction of unutilized reactant remaining. Thus, by measuring δ_0, δ_r, and δ_p, one can estimate the extent of the processes (f), or infer ε if unknown (Fig. I-3).

Because natural materials contain organic matter of diverse origin, their $\delta^{13}C$ or $\delta^{15}N$ are not suited for extracting information on the organisms of interest, such as f which reflect the physiological and environmental conditions. To understand the physiology of organisms and extract precise environmental information from natural samples, compound-specific isotope analysis has substantially developed in the last several decades. In particular, $\delta^{13}C$ and $\delta^{15}N$ of chloropigments and their degradation products, porphyrins, are among the most successful applications, because they derive exclusively from phototrophs inhabiting the photic zone and thus are not contaminated by other biological sources, unlike most of the other organic compounds.

Because the isotopic fractionations associated with the formation of chloropigments from the source C and N are constant in most cases, $\delta^{13}C$ and $\delta^{15}N$ of chloropigments and porphyrins can be calculated into those of source phototrophs; chlorophyll *a* is depleted in ^{15}N relative to the cell of eukaryotic algae by 4.8 ± 1.4‰ (± 1σ) (Sachs et al., 1999; Ohkouchi et al., 2006), and its degradation counterpart, deoxophylloerythroetioporphyrin (DPEP), enriched in ^{13}C relative to the cell of eukaryotic algae by 1.8 ± 0.8‰ (± 1σ) (Ohkouchi et al., 2008). The isotopic compositions of the estimated cell can then be

interpreted in the context of kinetic isotopic fractionation model described above.

Despite their usefulness, only few studies have applied this technique, because these measurements require time-consuming and tedious analytical procedures for isolation and purification, and also require sensitivity-enhanced device for the measurement of $\delta^{15}N$ of purified compounds (Ogawa et al., 2010). Thus, data presented in this work are not only useful as a proxy, but also important as contributing to the accumulation of knowledge on the isotopic distribution of chloropigments produced in various environmental settings, which would greatly help future researches applying the compound-specific isotope analysis of chloropigments.

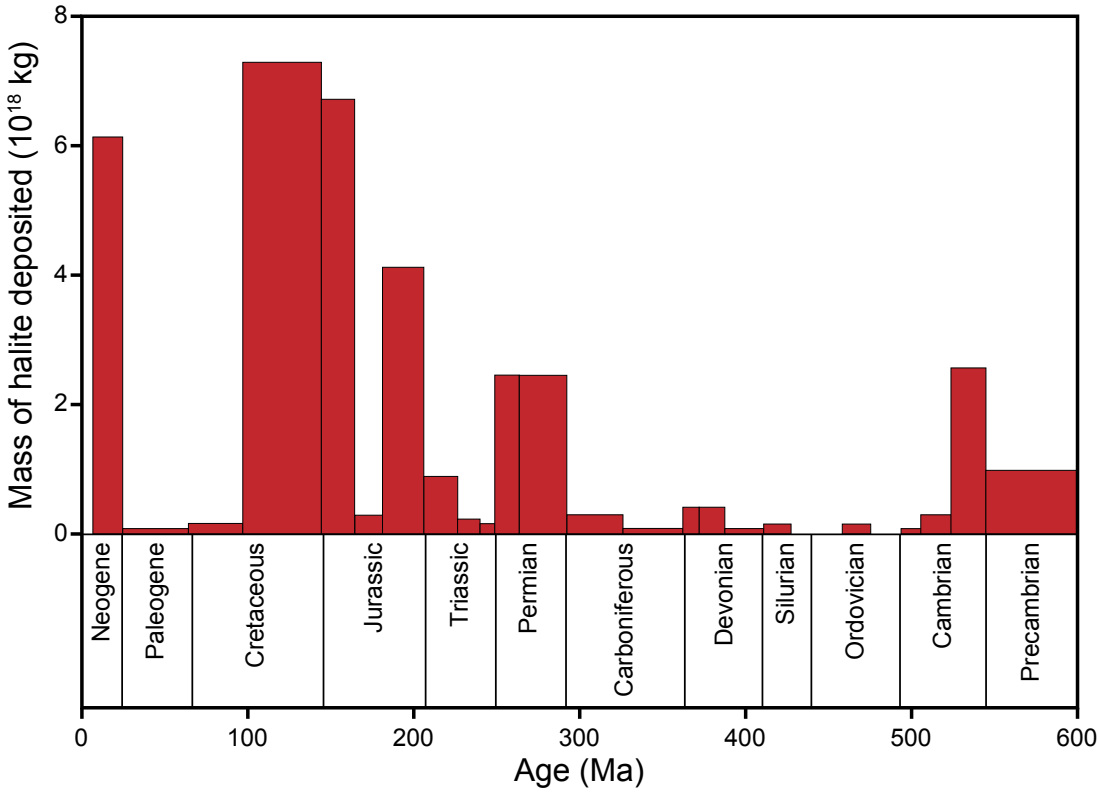

Fig. I-1. The maximum values of the masses of existing halite deposits through the Phanerozoic. Modified after Hay et al. (2006).

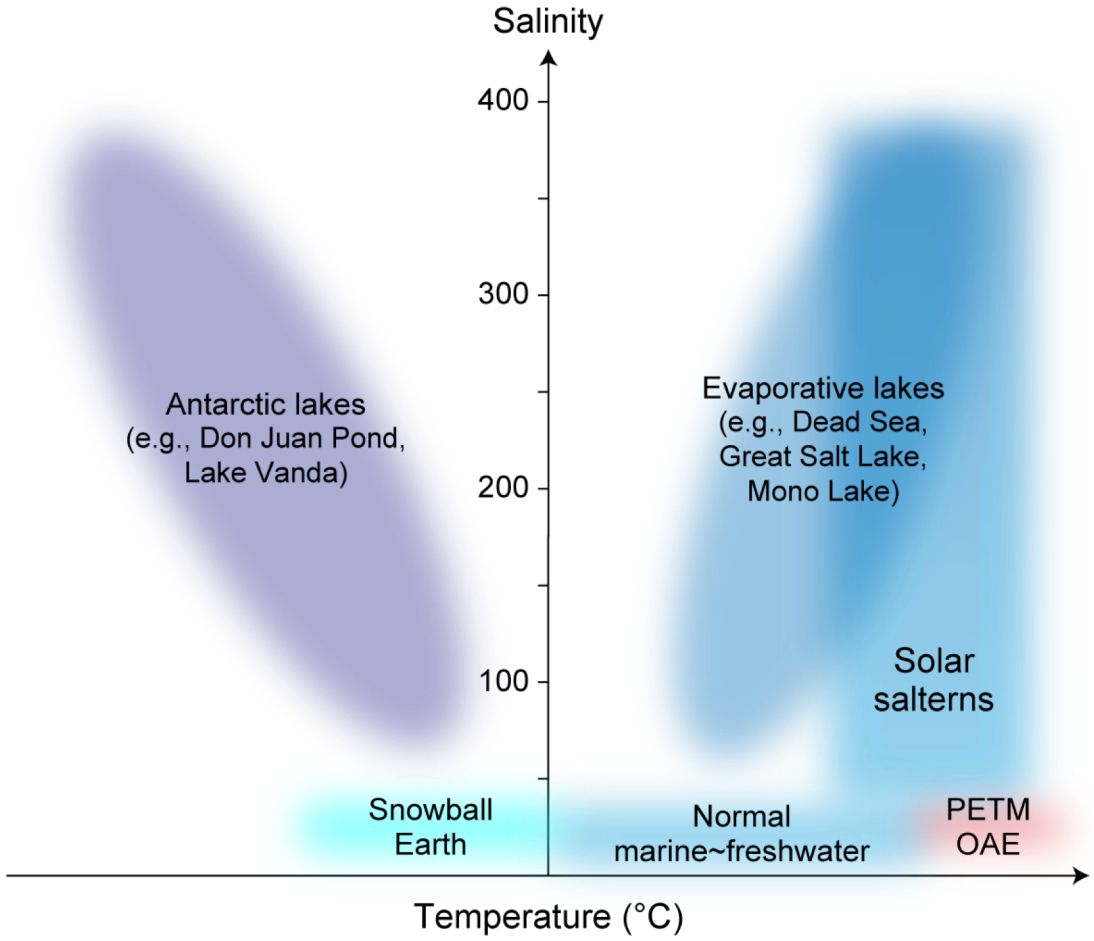

Fig. I-2. The temperature–salinity range of the modern hypersaline environments and the past extreme climatic events. PETM, Paleocene–Eocene Thermal Maximum; OAE, Cretaceous Oceanic Anoxic Event.

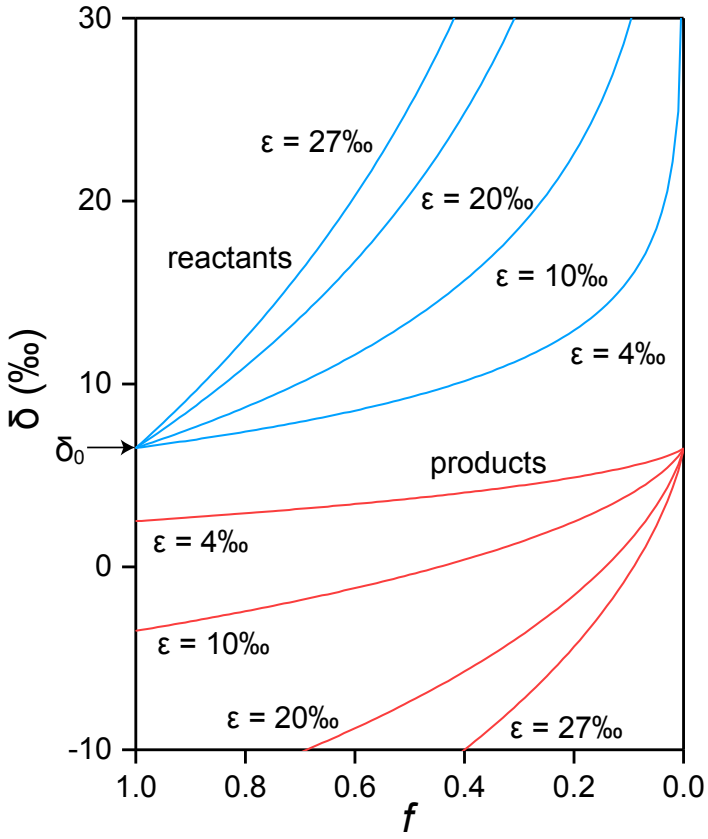

Fig. I-3. The isotopic compositions of the unutilized reactants (blue lines) and products (red lines) during kinetic isotopic fractionation as a function of the fraction of unutilized substrate (*f*). Curves are drawn for ε = 4, 10, 20, and 27‰.

CHAPTER II

THE CARBON CYCLE IN THE MODERN SHALLOW HYPERSALINE ENVIRONMENTS

II-1. Introduction

Although salinity is potentially a strong limiting factor of habitability, hypersaline environments are populated by a surprising diversity of microorganisms, especially in shallow settings, where benthic microbial mats form (e.g., Oren, 2002; Ley et al., 2006). It therefore follows that various biological processes are actively operating in the shallow hypersaline environment, strongly influencing the biogeochemical cycles and chemical characteristics of the system. In addition, seawater evaporation induces transitions in the state and composition of the microbial community through changes in various environmental factors (e.g., salinity, temperature, *p*H, light conditions). These changes result in modifications of the biological processes, which in turn strongly affect the environment. For these reasons, the chemical characteristics of the evaporating seawater are determined not only by physical and chemical processes induced by evaporation, but also by biological processes within the system. In this chapter, I focused on the solar salterns of Trapani (Sicily, Italy) to increase our understanding of the mutual interaction between physical, chemical, and biological processes with increasing salinity in hypersaline environment.

Solar salterns consist of a series of shallow ponds, normally less than 1 m deep, affording a large surface area for evaporation, with salinity increasing from seawater up to the saturation point of halite (NaCl). Different types of evaporite minerals precipitate on the bottom of the ponds according to the degree of evaporation (Logan, 1987; Geisler-Cussey, 1997). Calcium carbonate ($CaCO_3$, calcite or aragonite) starts to precipitate in ponds in which the evaporation of the original seawater exceeds 50%. When over 80% of the original seawater has been removed by evaporation, gypsum ($CaSO_4 \cdot 2H_2O$) starts to precipitate. Benthic microbial mats usually form in the salinity range within which calcium carbonate and gypsum precipitate. Halite starts to precipitate when evaporation

exceeds 90% of the original seawater. Various K–Mg salts start to precipitate after halite when the seawater is concentrated ~70 times. There is no benthic microbial community in these highly evaporated ponds, but there are planktonic microorganisms in halite crystallizer ponds (e.g., Antón et al., 2000; Řeháková et al., 2009). The evaporation changes not only the chemical composition but also the physical properties of the brine. For example, it decreases the solubility and diffusion of dissolved inorganic carbon (DIC; Raven, 1991) and changes the activity coefficients of ions through increasing ionic strength (Karcz and Zak, 1987).

One particular characteristic of these shallow hypersaline environment is the formation of a highly productive microbial mat. The hypersaline microbial mats formed at the bottom of the ponds are inhabited by highly diverse groups of microorganisms: cyanobacteria (e.g., Green et al., 2008), chemotrophic and phototrophic sulfur-oxidizing bacteria (e.g., Ollivier et al., 1994; Imhoff, 2001), and sulfate-reducing bacteria (e.g., Risatti et al., 1984; Canfield and Des Marais, 1993; Teske et al., 1998; Baumgartner et al., 2006). These groups are dominant in many of the hypersaline microbial mats at various sites, and together with less abundant but highly diverse groups of microorganisms they form a complex community structure. This extreme diversity is produced by the broad niche space provided by the light gradient and varying chemical conditions within the mat, which itself is modified by biological processes of the microorganisms (Ley et al., 2006).

Carbon, sulfur, and oxygen cycles within the mat clearly illustrate the mutual interaction among the microbial communities via biological modification of the chemical conditions (Van Gemerden, 1993). For example, primary production by photoautotrophs generates the organic carbon that fuels the entire ecosystem, but at the same time releases oxygen, which is toxic to anaerobes. The fixed carbon is degraded by fermenters and

mineralized to DIC by heterotrophs, sulfate-reducing bacteria and, in some cases, methanogens (e.g., Van Gemerden, 1993; Orphan et al., 2008). This efficient recycling of carbon inside the mat accounts in part for its high primary productivity (e.g., Canfield and Des Marais, 1993; Des Marais, 2003). On the other hand, sulfide produced by sulfate reduction is toxic to aerobic microorganisms, but is oxidized back to sulfate, biotically by chemotrophic and phototrophic sulfur bacteria and abiotically by oxygen produced during photosynthesis (e.g., Revsbech et al., 1983; Fründ and Cohen, 1992; Canfield and Des Marais, 1993). The activity of these biological processes fluctuates on a daily cycle controlled by light availability (e.g., Canfield and Des Marais, 1993).

Because most hypersaline evaporative settings in natural environments harbor a microbial community, it is of critical importance to understand the responses of biological processes to increasing salinity. As described above, the physical and biological processes associated with the evaporation of seawater have the potential to affect essential elements such as carbon, nitrogen, oxygen, and sulfur. Here, I specifically focus on changes in the carbonate system, which constitutes a fundamental part of the biogeochemical cycle and is an essential component of the Earth's climate system. The amount and chemical form of DIC, which is a resource for autotrophs, play a key role in biological processes. DIC concentrations in continental aquatic systems are maintained by water–atmosphere CO_2 exchange, precipitation and dissolution of minerals, photosynthesis, respiration, and external inputs such as soil CO_2 (e.g., Lazar and Erez, 1992). There are distinct inorganic and biological controls on the carbon budget and the relative proportions of the three major dissolved carbon forms—aqueous carbon dioxide ($CO_2(aq)$), bicarbonate (HCO_3^-), and carbonate ion (CO_3^{2-})—in an aquatic system. Thus, the interplay between changes in precipitating salts and microbial communities is key to understanding the changes in the carbonate system during evaporative concentration processes.

Here, I focused on the chemical compositions as well as the concentration and isotope signatures of DIC in salterns, with the aim of gaining a comprehensive understanding of carbon dynamics in the shallow hypersaline environment. I also investigated changes in primary productivity along the salinity gradient by performing compound-specific isotope analysis of photosynthetic pigments. The resulting insights are expected to also be beneficial as basic information for understanding the past massive evaporation events.

II-2. Materials and Methods

II-2.1. Study site

Three commercial solar salterns located in Trapani (Western Sicily, Italy) were studied: the Sosalt (SS), Culcasi (CU), and Chiusicella (CH) salterns (Fig. II-1). These solar salterns, each consisting of multiple ponds with different salinities, differ in scale; Sosalt is the largest, with a total surface area of 800 ha and an annual production of salt reaching 1×10^5 tons, and Chiusicella is the smallest in both surface area (7 ha) and number of ponds.

Progressively increasing salinities characterize each series of ponds, and the corresponding evaporite minerals that precipitate at the bottom. The ponds where calcium carbonate precipitates (carbonate ponds) are characterized by the formation of a dense benthic microbial mat. This microbial mat consists of a slimy layer a few millimeters thick, which is composed of thin yellow, green, and pink layers on the surface, and black, loose deposits buried underneath (Fig. II-2a, b). The gypsum ponds have a thick layer of gypsum precipitates, which consists of striking stratified solid layers of different colors—yellowish transparent, green, and pink layers, from the surface of the precipitate to a depth averaging around 5 cm—with loose black deposits below (Fig. II-2c, d). Large halite crystals (Fig. II-2e, f) form in the subsequent halite ponds. There are apparently no benthic

microbial communities in the halite ponds.

II-2.2. Sampling protocols

Normal seawater, brine, and deposits in the ponds were collected during the daytime in September 2015 (Table II-1). Seawater and brine samples were collected in 100-mL polyacrylonitrile (PAN) bottles. Those samples collected for the measurement of total alkalinity (TA), DIC concentration, and DIC carbon isotopic composition ($\delta^{13}C_{DIC}$) were immediately poisoned with 200 μL of saturated $HgCl_2$ solution to prevent further biological activity. The lid was closed without headspace until the analysis to prevent further gas exchange with the atmosphere. The temperature and *p*H of brine and seawater were measured in situ using a *p*H meter with a combination electrode (GST-5741C; DKK-TOA Corporation, Tokyo, Japan). The effect of temperature on *p*H was calibrated using the equation of Gieskes (1969). The *p*H values are given using the seawater hydrogen ion (SWS) scale. Brine and seawater samples were kept cool in a refrigerator until analysis.

Samples of pond deposits were collected by hand or by using a hammer and chisel. Microbial mats were collected from three ponds (SS-3, CU-1, and CU-2); small gypsum crystals were found in the deposits from SS-3. Gypsum crusts were collected from three ponds (SS-1, SS-2, and CH-1), and halite crystals from two ponds (SS-4 and CU-5). Samples were stored in a freezer until analysis.

II-2.3. Brine and seawater sample analysis

II-2.3.1. Salinity

Salinity was measured by using a digital laboratory salinometer at the National Institute of Advanced Industrial Science and Technology, Japan (AIST) (Digi-Auto model 5, Tsurumi-Seiki Co., Kanagawa, Japan). Standard seawater (International Association

for the Physical Sciences of the Ocean [IAPSO]) was used as a reference. Analytical precision was within ±0.01 salinity unit.

II-2.3.2. Ion concentrations

Brine samples were diluted on a weight basis with ultrapure water prior to analysis. Concentrations of Na^+, Mg^{2+}, and K^+ were measured by ion chromatography at the Japan Agency for Marine-Earth Science and Technology (JAMSTEC) (Dionex ICS-1600, Thermo Fisher Scientific, Inc., Waltham, Massachusetts, USA), as were Cl^-, Br^-, and SO_4^{2-} (Dionex ICS-2100, Thermo Fisher Scientific, Inc.). Elemental boron (B) and Ca^{2+} were measured using inductively coupled plasma-optical emission spectrometry at JAMSTEC (ICP-OES, SII SPS5510, SII NanoTechnology Inc., Chiba, Japan). The analytical precisions (± 2σ) of replicate measurements were within ±2% for Na^+ and Cl^-, and ±10% for the other elements.

II-2.3.3. Total alkalinity

Total alkalinity was measured using a total alkalinity titrator at AIST (ATT-05, Kimoto Electric Co., Osaka, Japan). Samples were titrated with 0.1 M HCl, and TA was calculated by the Gran method. Samples collected from CH-1, SS-4, and CU-5 were diluted on a weight basis with ultrapure water prior to the measurement. The analytical precision of replicate measurements was within ±1.5%.

II-2.3.4. DIC concentration and carbon isotopic composition

For measurement of DIC, brine samples (10–50 mL) were transferred to a glass vial, and the air inside was completely evacuated using a high-vacuum glass line. Next, the samples were reacted with H_3PO_4 and left for 12 h so that DIC was completely converted

to CO_2 gas. The evolved gas was then introduced into a high-vacuum glass line and separated cryogenically. The gas pressure in the glass line was recorded and converted to DIC concentration. The precision of the DIC measurement was within 0.3%. Afterwards, the purified CO_2 gas was introduced into an isotope-ratio mass spectrometer (Delta Plus XL, Thermo Fisher Scientific, Inc.) to measure the carbon isotopic composition of the DIC. Isotopic compositions are expressed as conventional $\delta^{13}C$ relative to Vienna Pee Dee Belemnite. The analytical precision was within 0.1‰.

II-2.4. Deposit sample analyses

II-2.4.1. Composition of evaporites in the deposits

To estimate the amount of gypsum precipitated in the carbonate ponds CU-1 and CU-2, powder X-ray diffraction analysis (XRD; X'Pert Pro, PANalytical B.V., Almelo, The Netherlands) was conducted on the deposits of these ponds. Powdered standard materials of calcite and gypsum were prepared, and calcite–gypsum mix standard for the calibration curve (calcite/[calcite+gypsum] = 0.1, 0.3, 0.5, 0.6, 0.7, 0.8, 0.9 on weight basis) were made. The deposits of the ponds CU-1 and CU-2 were washed with methanol and dried completely, and then powdered using agate mortar. The analytical precision was calculated based on three replicate measurements for each sample and standard.

II-2.4.2. Carbon isotopic composition of sediment TOC

Sediment samples collected from the bottom of the ponds were subsampled for measurement of $\delta^{13}C$ of the bulk organic matter ($\delta^{13}C_{TOC}$). Samples collected from the carbonate ponds were separated into two parts: the upper slimy layer and the loose black deposit underneath (Fig. II-2b). The gypsum crusts were separated into four parts: the yellowish transparent, green, and pink gypsum layers, and the loose black deposits below

(Fig. II-2d). Subsampled deposits were freeze-dried and ground to powder. Together with ground halite samples, they were transferred to pre-cleaned smooth-wall tin capsules and treated with 0.1 M HCl to remove $CaCO_3$. After the samples were dried they were analyzed for $\delta^{13}C_{TOC}$ at JAMSTEC using a modified Flash EA1112 automatic elemental analyzer connected to a Thermo Finnigan Delta plus XP isotope ratio mass spectrometer (IRMS) via a ConFlo III Interface (Ogawa et al., 2010). Isotopic compositions are expressed as conventional $\delta^{13}C$ values relative to Vienna Pee Dee Belemnite. The analytical precision ($\pm 1\sigma$) was within 0.3‰.

II-2.4.3. Compound-specific pigment isotopic composition

The surface deposits from CU-1 and SS-3 (microbial mat), the yellowish transparent, green, and pink layers from SS-1 and CH-1 (gypsum crust), and halite crystals from SS-4 and CU-5 were analyzed for compound-specific isotope compositions of pigments. First, the deposits were freeze-dried and ground to powder. Organic matter was extracted with acetone three times by sonication for 15 min in an ultrasonic ice bath. The acetone fraction was then extracted with *n*-hexane three times. The *n*-hexane fraction was dried completely under N_2 gas and dissolved in 100 μL of *N*,*N*-dimethylformamide for high-performance liquid chromatography (HPLC) injection. All procedures were carried out in a dark room.

Pigment isolation and purification was accomplished using dual step HPLC. The HPLC system comprised a binary pump (G1312B; Agilent, Santa Clara, California, USA), an on-line degasser (G1379B; Agilent), an autosampler (G1367C; Agilent), a column temperature controller (Cool Pocket Column Chiller; Thermo Fisher Scientific), an on-line photodiode-array detector (G4212B; Agilent), and a fraction collector (G1364C; Agilent). The pigments were isolated using an Agilent Zorbax Eclipse XDB C-18 column (4.6 mm × 250 mm; 5 μm silica particle size) with a guard column (4.6 mm × 12.5 mm;

5 μm silica particle size). The pigments were eluted isocratically with 75% acetonitrile: pyridine (100:0.5, v/v) and 25% ethyl acetate: pyridine (100:0.5, v/v) for 5 min, followed by a linear gradient of ethyl acetate: pyridine to 50% over 50 min. The flow rate was set to 1 mL min^{-1} and the column temperature to 30 °C. Pigments were detected by the photodiode-array detector. The structure assignment of each compound was accomplished by comparing the photoabsorption spectra and the retention times with those of authentic standards. Chlorophyll *a* (Chl *a*), bacteriochlorophyll *a* (BChl *a*), and β-carotene were collected using the fraction collector. The entire peak was carefully collected for each compound to avoid analytical isotopic fractionation.

The collected pigments were dried completely under argon gas. Prior to the second HPLC purification step, Chl *a* and BChl *a* were dissolved in 1.5 mL hexane and reacted with 2 M HCl to convert them to pheophytin *a* (Pheo *a*) and bacteriopheophytin *a* (BPheo *a*), respectively. The hexane fraction was collected and dried completely under argon gas, and dissolved in 100 μL of *N*,*N*-dimethylformamide for HPLC injection. The column used for second purification step was an Agilent Zorbax Eclipse PAH column (4.6 mm × 250 mm; 5 μm particle size). Pigments were eluted isocratically with 80% acetonitrile: pyridine (100:0.5, v/v) and 20% ethyl acetate: pyridine (100:0.5, v/v) for 5 min, followed by a linear gradient of ethyl acetate: pyridine to 60% over 25 min, and a linear gradient of ethyl acetate: pyridine to 100% over 10 min. The flow rate was set to 1 mL min^{-1} and the column temperature to 15 °C.

The stable carbon isotopic compositions of the pigments were measured using a modified EA/IRMS (Ogawa et al., 2010). Purified pigments were dissolved in dichloromethane, transferred to pre-cleaned smooth-wall tin capsules, and dried before analysis. The analytical precisions (± 1σ) were within 0.3‰ for Chl *a* and BChl *a*, and 0.6‰ for β-carotene.

II-3. Results

Data from the brine sample analyses are summarized in Tables II-1 and II-2. The brines in the solar salterns originate from seawater from the same region, and precipitation of evaporites is the major process occurring within the salterns. Thus, I report and discuss the data from different solar salterns together, under the assumption that the biological processes in the three systems are comparable. I did not determine the salinity or the concentration of Na^+ and Cl^- of the brine samples collected from the ponds with higher salinities (CH-1, SS-4, and CU-5) because halite crystals precipitated in the sample bottles after the samples were collected.

II-3.1. Variations in concentrations of inorganic elements

The concentrations of solutes in the brines are determined mainly by condensation due to evaporation, removal by precipitation of evaporite minerals, and the effects of biological activity. One way to determine the behavior of the solutes is to normalize their concentrations by the degree of evaporation (DE: e.g., Bąbel and Schreiber, 2014). The DE of the brine can be estimated from the concentrations of the solutes that behave conservatively upon evaporation. In the salinity range of my samples, Mg^{2+}, K^+, Br^-, and B behave as conservative solutes. Here, I estimated the DE of each brine sample from the Mg^{2+} concentration as follows:

$$DE_{Mg} = \frac{[Mg^{2+}_{brine}]}{[Mg^{2+}_{seawater}]}$$

where $[Mg^{2+}_{seawater}]$ and $[Mg^{2+}_{brine}]$ are the molar concentrations of Mg ions in the seawater and brine samples, respectively. Normalization of the solute concentrations by DE_{Mg} cancels out the effect of condensation due to evaporation, therefore allowing the examination of the addition or removal of solutes to or from the brine.

The composition of the major ions in the sample of seawater (CU-0), which is the source of the brines in the solar salterns studied, was comparable to that reported for average modern seawater (Bąbel and Schreiber, 2014). The major evaporite minerals precipitated from seawater in the salinity range of my samples are calcium carbonate, gypsum, and halite. Accordingly, ions such as Ca^{2+}, HCO_3^-, SO_4^{2-}, Na^+, and Cl^- are removed sequentially from the seawater (Fig. II-3, Table II-2). To evaluate the process of the precipitation of evaporites in the Trapani solar salterns, my results were compared with computer-modeled concentration curves, which are calculated by assuming an absence of biological activity. Specifically, the calculations of Timofeeff et al. (2001) were used, in which the back-reaction between the brine and evaporites is inhibited to simulate more realistically the evaporation process in solar salterns. Major ions plotted against each other lie on the line of the modeled evaporation curves (Fig. II-4), indicating that, for these major ions, seawater in the solar salterns apparently follows an evaporation path with no influence from biological activity.

II-3.2. Composition of evaporites in the deposits of the carbonate ponds

The XRD patterns of the mix standard materials showed peaks attributable to calcite and gypsum. Their peak heights changed consistently in response to changes in the proportion of each mineral (Fig. II-5a). The highest peaks of calcite and gypsum were selected, and peak height ratios were calculated for drawing the calibration curve, which was fitted with second polynominal approximation line (Fig. II-6). The peak height ratios of deposits in CU-1 and CU-2 were calculated into the content ratio of calcite (calcite/[calcite+gypsum]) using the calibration curve, which were 0.34–0.40 and 0.10–0.15, respectively (Fig. II-5b, II-6). Thus, although CU-1 and CU-2 are considered as “carbonate ponds”, small amount of gypsum is already precipitating. Precipitation of

gypsum in part accounts for small decreases in $[Ca^{2+}]/DE_{Mg}$ and $[SO_4^{2-}]/DE_{Mg}$ from seawater to CU-2.

II-3.3. Variations in carbonate system parameters

DIC concentrations decreased from the seawater value of 2.04 mmol L^{-1} to 1.00 mmol L^{-1} in the carbonate ponds, and then increased to 5.95 mmol L^{-1} in the halite ponds (Fig. II-7, Table II-1). When normalized by DE_{Mg}, there was a sharp drop from seawater to the carbonate ponds. Variations in $[DIC]/DE_{Mg}$ were relatively small in the subsequent ponds. TA increased progressively from the seawater value of 2.68 mmol L^{-1} to as high as 21.1 mmol L^{-1} in the halite pond. In highly evaporated brine, a substantial portion of TA originates from boric acid (Golan et al., 2016), which behaves conservatively upon evaporation. Variations in $[TA]/DE_{Mg}$ followed the same trend as that of $[DIC]/DE_{Mg}$ because increases in TA due to accumulating boric acid are canceled out upon normalization. Similar variations in DIC and TA along a salinity gradient have been reported in the solar saltern of Eilat, Israel (Lazar and Erez, 1992).

Interestingly, $\delta^{13}C_{DIC}$ was highly variable during the course of evaporation (Fig. II-7). It decreased substantially from the seawater value of 2.2‰ and remained low through the gypsum ponds, with a minimum of –10.6‰. There was subsequently a substantial increase in the halite ponds to the highest value of 7.2‰ (DE_{Mg} = 22.0). Lazar and Erez (1992) also reported this pattern of variation in $\delta^{13}C_{DIC}$ with increasing salinity.

Seawater *p*H measured at the intake of the pond system was 8.2 and increased to 8.5 in the carbonate ponds in which there was a microbial mat (Fig. II-7). It then decreased gradually to reach 7.0 in the halite ponds.

II-3.4. Organic carbon isotopic composition ($\delta^{13}C_{TOC}$) of deposits

Values of $\delta^{13}C_{TOC}$ were high compared to the values in normal marine settings, and decreased from a maximum of –8.6‰ in the carbonate ponds to a minimum of –22.7‰ in the halite ponds (Fig. II-8, Table II-3). The differences between $\delta^{13}C_{TOC}$ and $\delta^{13}C_{DIC}$ increased as the salinity increased. Depth profiles of $\delta^{13}C_{TOC}$ do not show any common trends among ponds (Fig. II-9, Table II-3). The lack of a common trend may be because the isotopic signals of organisms living in the lower layers of the deposits are superimposed on the signals of upper-layer organisms, reflecting the fact that the lower-layer deposits consist of upper-layer deposits that subsequently became buried and then occupied by lower-layer dwellers.

II-3.5. Distribution of pigments and their carbon isotopic composition

The distribution of pigments was similar for the same types of samples from different solar salterns. Therefore, only representative chromatograms are shown: from the surface slimy layer of the microbial mats in the carbonate ponds, from the yellowish transparent, green, and pink layers of the gypsum crusts in the gypsum ponds, and from the halite crystals in the halite ponds (Fig. II-10).

The major pigments detected in the surface slimy layer of the carbonate ponds were the Chl *a* series, the BChl *a* series, and various carotenoids. The Chl *a* series includes Chl *a* and its degradation products, Pheo *a* and pyropheophytin *a* (PPheo *a*). The BChl *a* series includes BChl *a* and its degradation products, BPheo *a* and bacteriopyropheophytin *a* (BPPheo *a*). Among the various carotenoids detected, the peaks with a retention time around 23 min were identified as β-carotene and its degradation products (β-carotene series), based on a comparison with the authentic standard. The relative concentrations of the original pigments (i.e., Chl *a* and BChl *a*) were substantially higher than their

counterpart degradation products. Thus, the $\delta^{13}C$ of Chl *a*, BChl *a*, and β-carotene were measured.

In the gypsum crust, the main pigments in the yellowish transparent layer and the green layer were the Chl *a* series and smaller peaks of carotenoids, including the β-carotene series. The pink layer contained Chl *a*, BChl *a*, and the β-carotene series, with BChl *a* highest in concentration. The Chl *a* in the pink layer was probably originally from the cyanobacteria or algae in the upper yellowish and green layers, because they migrate upward as the photic and oxic zones moves upward with the growth of the gypsum crust. Therefore, $\delta^{13}C$ of Chl *a* in the yellowish transparent layer and the green layer, which is dominated by cyanobacteria and algae, and BChl *a* in the pink layer dominated by purple sulfur bacteria were measured. $\delta^{13}C$ of β-carotene in the yellowish transparent layer of the gypsum crust were also measured.

The pigment distribution in the halite crystals from the halite ponds was completely different from that in the carbonate and gypsum ponds, with the β-carotene series in highest concentrations and extremely low Chl *a* concentrations. Because there was not enough Chl *a* for isotopic measurement, only the $\delta^{13}C$ values of the β-carotene series were determined in halite samples.

The depth variations of pigment $\delta^{13}C$ values showed similar patterns in all ponds: $\delta^{13}C$ of BChl *a* was lower than that of Chl *a* in both microbial mats and gypsum crusts (Fig. II-9, Table II-4). In a comparison between ponds, the $\delta^{13}C$ values of Chl *a*, BChl *a*, and β-carotene were highest in CU-1, at –11.5‰, –19.5‰ and –22.1‰, respectively (Fig. II-8). The $\delta^{13}C$ values of all pigments showed decreasing trends as evaporation proceeded, and reached minimum values of –20.6‰ and –26.3‰ in CH-1 for Chl *a* and BChl *a*, respectively, and –28.5‰ in CU-5 for β-carotene. The $\delta^{13}C_{TOC}$ of the surface sediment samples showed similar trends.

An isotopic fractionation factor was calculated from the $\delta^{13}C_{DIC}$ in the surface brine and that of TOC, Chl *a*, and β-carotene defined as follows:

$\varepsilon \equiv (R_{org}/R_{DIC}) \times 10^3$ (‰)

where R_{org} is $^{13}C/^{12}C$ for TOC, Chl *a*, or β-carotene. The $\delta^{13}C$ of Chl *a* and β-carotene originating from the surface slimy layer of the microbial mats, the yellowish transparent layer from the gypsum crusts, and the halite crystals were used for the calculation, which contain pigments derived from microorganisms assumed to assimilate DIC mainly from the surface brine. Overall, the values of ε were lower in the lower salinity ponds, and increased more or less linearly as evaporation proceeds (Fig. II-8). Between TOC, Chl *a*, and β-carotene, ε of β-carotene was highest, ranging from 14.9‰ to 36.0‰, followed by that of Chl *a*, ranging between 6.4‰ and 17.3‰, and the lowest, that of TOC, ranging from 3.5‰ to 30.2‰.

The concentration of each pigment was not quantified because of the somewhat patchy distribution of the colored layers on the pond bottoms. However, the rough estimates indicate that the concentrations of Chl *a* and BChl *a* were on the order of micrograms per gram of dry sediment for the microbial mat and the gypsum crust.

II-4. Discussion

II-4.1. Changes in primary production with increasing salinity

For estimating the primary productivity, the $\delta^{13}C$ of pigments has an advantage over $\delta^{13}C_{TOC}$ because the pigments derive exclusively from photoautotrophs; thus, other factors such as heterotrophic activity, which potentially affects $\delta^{13}C_{TOC}$, are excluded.

Among the pigments measured in this study, Chl *a* and β-carotene are synthesized by aerobic photoautotrophs such as cyanobacteria and algae, and BChl *a* is produced by the purple sulfur bacteria present in the pink layer of the microbial mat. Because

cyanobacteria dominate over eukaryotic algae in the microbial mats of the solar salterns worldwide (e.g., Oren, 2002; Airs and Keely, 2003; Green et al., 2008), I assumed that the chlorophyll *a* originated mainly from cyanobacteria. Both planktonic and benthic phototrophs are generally present in the solar salterns. In Spain, the reported concentrations of Chl *a* in the brine of a solar saltern were around 2–15 μg L^{-1} (Joint et al., 2002). On the other hand, the concentrations of Chl *a* in the benthic deposits of the Trapani solar salterns were on the order of micrograms per gram of dry sediment, which is much higher than the concentration of the overlying brine reported in Joint et al. (2002). Although the concentration of Chl *a* in the brine was not measured in this study, these observations indicate that the dominant primary producer is the benthic community in ponds where benthic microbial mat is formed. Chl *a* and β-carotene in the halite ponds originate from planktonic photoautotrophs, because these ponds contain no benthic microbial mat. Specifically, *Dunaliella salina* is the likely candidate, as this organism is known to be a dominant primary producer in halite ponds (e.g., Řeháková et al., 2009), and it also accumulates high amounts of β-carotene relative to chlorophyll *a* (Oren, 2005).

There are several possible factors that could account for the lower $\delta^{13}C$ of BChl *a* compared to that of Chl *a* in the benthic community (Fig. II-9). One is the difference in the source of DIC utilized by each photoautotroph. Because the purple sulfur bacteria inhabit the deeper layer of the mat, some proportion of DIC assimilated by them is supplied through mineralization of the organic matter within the mat. The values of $\delta^{13}C_{TOC}$ indicate that $\delta^{13}C$ of the mineralized DIC is lower than that of DIC in the surface brine, because isotopic fractionation associated with degradation of organic matter is negligible (e.g., Meyers and Eadie, 1993). Another factor is the chemical species of DIC assimilated by the photoautotroph. Cyanobacteria are capable of assimilating HCO_3^- through active transport (e.g., Kaplan et al., 1980; Badger and Price, 2003). Because

HCO_3^- is enriched in ^{13}C compared to CO_2(aq) by 8.4‰ under the temperature of 30 °C (Mook et al., 1974), active assimilation of HCO_3^- by cyanobacteria may have resulted in the relatively high $\delta^{13}C$ of Chl *a*. As for the purple sulfur bacteria, $\delta^{13}C$ depletion in BChl *a* compared to Chl *a* has been reported from the saline meromictic Lake Kaiike in Japan (Ohkouchi et al., 2005). Because purple sulfur bacteria, cyanobacteria, and algae use identical biochemical pathways for carbon assimilation and chlorophyll biosynthesis, differences in their $\delta^{13}C$ can be ascribed to physiological factors such as growth rate, cell size, or geometry (Pancost et al., 1997; Popp et al., 1998; Bidigare et al., 1999; Ohkouchi et al., 2008).

The isotopic fractionation factor (ε) calculated from Chl *a* and β-carotene increased almost linearly with increasing salinity (Fig. II-8). Because the source photoautotrophs of these pigments do not change substantially along the salinity gradient, there are several possible explanations for this observation. The habitat of the photoautotrophs is one of the major factors controlling ε along the salinity gradient, because while planktonic photoautotrophs such as *D. salina* inhabiting the halite ponds can utilize DIC in the surface brine, cyanobacteria inhabiting the surface of the microbial mats and gypsum crusts utilize DIC that diffuses from the overlying brine or from the lower part of the mat. DIC diffusion into the benthic microbial mat can be limited by a diffusive boundary layer over the mat surface (Jørgensen, 1994a) or within the mat (Wieland et al., 2001). As for the gypsum crust, there is likely only limited exchange of brine through the pore water. These limits on diffusion could result in DIC-limited conditions inside the microbial mat, which is expressed as a relatively small ε without depletion of DIC in the overlying brine. Indeed, limited DIC diffusion into the microbial mat has also been considered as a possible reason for relatively high $\delta^{13}C_{TOC}$ and therefore low values of ε (e.g., Des Marais and Canfield, 1994; Schouten et al., 2001). From this perspective, the relatively large ε in

the halite ponds is because the habitat of the dominant photoautotroph, *D. salina*, is in the surface brine, where conditions are not DIC-limited.

Another possible factor controlling ε along the salinity gradient comes from the observation that ε increases when compared among ponds of the same type: the carbonate ponds (CU-1, SS-3), the gypsum ponds (SS-1, CH-1), and the halite ponds (SS-4, CU-5). The only exception is the decrease in ε calculated from $\delta^{13}C$ of β-carotene in the carbonate ponds. If the diffusion rate of DIC into the mat or the crust does not change substantially with increasing salinity, then the increase in ε can be interpreted as reflecting a lower proportion of DIC assimilated by photoautotrophs under the higher salinities. In other words, increasing salinity may have suppressed primary production. This suggestion is consistent with the findings of previous studies that photosynthesis decreases with increasing salinity (Oren, 2009) in microbial mats (e.g., Pinckney et al., 1995; Wieland and Kühl, 2005) and gypsum crusts (e.g., Caumette et al., 1994; Canfield et al., 2004), as well as in the planktonic community of halite ponds (Joint et al., 2002). Salinity may directly control the primary productivity by affecting the physiology of photoautotrophs, or indirectly by affecting the elemental cycles of nutrients such as nitrogen, phosphorus, and iron.

II-4.2. Effect of biological activities on the chemical evolution of evaporating seawater

II-4.2.1. Influence of sulfate reduction on brine

One of the highest rates of sulfate reduction known occurs in hypersaline microbial mats (Canfield and Des Marais, 1991). Sulfate reduction removes SO_4^{2-} from brine by reduction to H_2S or HS^- and subsequent precipitation as various metal sulfides (e.g., Wieland et al., 2005; Valdivieso-Ojeda et al., 2014). Although this process must have

removed some portion of SO_4^{2-} from the brine in this study, concentrations of SO_4^{2-} plotted against other major ions lie on the line of the ideal curve (Fig. II-4). To evaluate the influence of the sulfate reduction in the brine, the amount of sulfate removed were roughly estimated on the basis of sulfate reduction rates in hypersaline microbial mats and gypsum crusts of the solar salterns of Guerrero Negro, Mexico (Canfield and Des Marais, 1991, 1993), Eilat, Israel (Fründ and Cohen, 1992; Jørgensen, 1994b; Canfield et al., 2004; Sørensen et al., 2004), and Salins-de-Giraud, France (Caumette et al., 1994). Assuming an average pond water depth of 50 cm, the amount of SO_4^{2-} reduced by 20 cm^2 of the mat was calculated, which corresponds to 1 L of overlying brine. The calculated value varied substantially for both the microbial mats and the gypsum crusts; both varied between tens of micromoles to millimoles per liter per day. In contrast, the SO_4^{2-} in the overlying brine in the Trapani solar salterns ranged from 79.2 to 233.2 mmol L^{-1} from the carbonate to the gypsum ponds.

Although sulfate reduction rates were not measured in the Trapani solar salterns, this rough estimation implies that sulfate reduction can influence the SO_4^{2-} concentration of the brine if the reduction is on the order of millimoles per liter per day. The fact that the SO_4^{2-} concentration tracks the ideal evaporation curve therefore indicates that SO_4^{2-} is supplied by other processes to compensate any loss through reduction, or that the sulfate reduction rate in the Trapani solar salterns is low. One possible source of SO_4^{2-} for the former explanation is oxidation of the reduced sulfur species by chemotrophic and phototrophic sulfur bacteria or by oxygen produced by photosynthesis in the upper layer of deposits and surface brine (e.g., Revsbech et al., 1983; Fründ and Cohen, 1992; Canfield and Des Marais, 1993). Note that decreases in SO_4^{2-} and increases in TA are canceled out by sulfide oxidation, but increases in DIC are not.

II-4.2.2. Effect of biological processes on the brine carbonate system

In the shallow hypersaline environment where benthic microbial mats form, carbonate system parameters, i.e., DIC, TA, *p*H, and pCO_2, are affected by various processes such as calcium carbonate precipitation and dissolution (Eq. II-1 below), photosynthesis and respiration (Eq. II-2), sulfate reduction (Eq. II-3), sulfide oxidation (Eq. II-4), and $CO_2(g)$ exchange with the atmosphere. The following equations describe these processes.

$$Ca^{2+} + 2HCO_3^- \rightleftarrows CaCO_3(s) + CO_2(g) + H_2O \quad \text{Eq. II-1}$$

$$106CO_2 + 16HNO_3 + H_3PO_4 + 122H_2O \rightleftarrows (CH_2O)_{106}(NH_3)_{16}(H_3PO_4) + 138O_2 \quad \text{Eq. II-2}$$

$$SO_4^{2-} + 2CH_2O \rightarrow HS^- + 2HCO_3^- + H^+ \quad \text{Eq. II-3}$$

$$HS^- + 2O_2 \rightarrow SO_4^{2-} + H^+ \quad \text{Eq. II-4}$$

The values for $[DIC]/DE_{Mg}$ and $[TA]/DE_{Mg}$ indicate that DIC and TA are removed from the brine during the course of evaporation from the seawater to the carbonate ponds, accompanied by a substantial drop in $\delta^{13}C_{DIC}$ (Fig. II-7). In this salinity range, calcium carbonate precipitation is one of the major process affecting DIC concentrations, decreasing the $\delta^{13}C_{DIC}$ of the brine by preferentially removing ^{13}C from DIC reservoirs. The typical enrichment factors for carbon isotope fractionation between calcium carbonate and DIC are +1.0‰ and +2.7‰ for calcite and aragonite, respectively (Romanek et al., 1992). Theoretically, the decrease in $\delta^{13}C_{DIC}$ in CU-1 from the seawater value of 2.2‰ to –5.1‰ could be reached if almost all DIC precipitated as calcium carbonate. However, calcium carbonate precipitation from seawater to $DE_{Mg} = 6.7$ results in a TA loss of around 60% of the source seawater, in the absence of biological activity (Lazar et al., 1983). Therefore, calcium carbonate precipitation alone cannot explain the drop in $\delta^{13}C_{DIC}$ from 2.2‰ to –5.1‰ (from seawater to CU-1) or from –5.1‰ to –10.6‰

(from CU-1 to CU-2).

DIC is affected by processes such as calcium carbonate precipitation and dissolution, photosynthesis and respiration, sulfate reduction, and CO_2(g) exchange with the atmosphere. On the other hand, TA is primarily affected by precipitation and dissolution of calcium carbonate, sulfate reduction, and sulfide oxidation. It was suggested in section II-4.2.1 that the loss of SO_4^{2-} through sulfate reduction was compensated for by sulfide oxidation, or that the rate of sulfate reduction was low. These observations imply that the net change in TA must have also been near zero. Cyanobacteria, the main photoautotroph in the hypersaline microbial mat, are capable of assimilating HCO_3^- during photosynthesis (e.g., Kaplan et al., 1980; Badger and Price, 2003). This process does not affect TA, however, because they release OH^- when utilizing HCO_3^- as the carbon source (Prins and Elzenga, 1989).

On the basis of these observations, the amount of calcium carbonate precipitated was calculated from the changes in TA, taking the transition from CU-0 (seawater) to CU-1 (DE = 2.7) as the model case. It is calculated that 1.40 mmol L^{-1} of TA is lost from the seawater to CU-1. According to Eq. II-1, the precipitation of one mole of calcium carbonate utilizes two moles of HCO_3^- and releases one mole of CO_2(g). The buffering effect of seawater reduces the actual amount of CO_2(g) liberated to the atmosphere to around 0.6 mole per mole of calcium carbonate precipitated (Ware et al., 1992; Frankignoulle et al., 1994). Under the assumption that this rule is applicable to the hypersaline solutions in saltern ponds, 1.40 mmol L^{-1} of TA loss is equivalent to the precipitation of 0.70 mmol L^{-1} calcium carbonate and production of 0.70 mmol L^{-1} of CO_2(g), of which 0.28 mmol L^{-1} is re-dissolved into the solution, during the transition from seawater to the brine in CU-1. This results in a decrease of 1.12 mmol L^{-1} of DIC, because calcium carbonate precipitation decreases DIC and TA equally but the re-

dissolution of CO_2(g) increases only DIC. However, the actual decrease in DIC from CU-0 to CU-1 was 1.57 mmol L^{-1}, according to the changes from seawater to CU-1. This value indicates that 0.45 mmol L^{-1} of DIC was lost by processes other than calcium carbonate precipitation (Fig. II-11).

There are several possible processes responsible for the loss of DIC other than calcium carbonate precipitation. One is carbon fixation by photoautotrophs, which preferentially removes ^{13}C-depleted DIC from the brine. The isotopic fractionation factor (ε) calculated from the $\delta^{13}C$ of pigments indicates that photosynthesis was more active in the lower salinity ponds (Fig. II-8). The degassing of CO_2(aq) due to a decrease in solubility induced by evaporation also removes ^{13}C-depleted DIC from the brine (Li and Tsui, 1971; Stiller et al., 1985; Raven, 1991; Barkan et al., 2001). This process was active throughout the evaporation path. Thus, although these processes that remove ^{13}C-depleted DIC from the brine could balance the DIC budget, there must be other processes supplying ^{13}C-depleted DIC to explain the ^{13}C-depleted $\delta^{13}C_{DIC}$ of the carbonate ponds. I propose several processes that may account for the supply of ^{13}C-depleted DIC:

(1) Because intensive photosynthesis and degassing due to evaporation remove CO_2(aq) from the brine, some DIC must have been supplied by equilibrium with atmospheric CO_2, which is relatively depleted in ^{13}C (e.g., Keeling, 1958). Moreover, Baertschi (1952) suggested that ^{13}C-depleted CO_2 might be selectively dissolved into brine from the atmosphere under alkaline conditions ("the Baertschi effect"). As also suggested by Lazar and Erez (1992), this process may be responsible for the ^{13}C-depleted DIC in the brine of the carbonate ponds.

(2) A previous study excluded sulfate reduction releasing DIC in the form of HCO_3^- as the main cause of relatively low $\delta^{13}C_{DIC}$ of the brine because there was no substantial increase in [TA]/DE_{Mg} with increasing DE_{Mg} (Fig. II-7; Lazar and Erez,

1992). In the Trapani solar salterns, the changes in SO_4^{2-} concentration suggest that the loss of SO_4^{2-} through sulfate reduction was compensated for by sulfide oxidation, or else the rate of sulfate reduction was low (Fig. II-4). As suggested in section II-4.2.1, sulfate reduction coupled with sulfide oxidation cancels out increases in TA, but not DIC. Therefore, the possibility that the ^{13}C-depleted DIC was supplied by sulfate reduction cannot be excluded. It may originate from the benthic microbial mat within the pond, or from the highly productive microbial communities in less evaporated, upstream ponds (Joint et al., 2002). Note that the actual amount of DIC that diffuses into the overlying brine is less than the amount mineralized from organic matter, because of restricted diffusion of DIC within the mat (Wieland et al., 2001) and on the mat surface (Jørgensen, 1994a). Indeed, Canfield and Des Marais (1993) suggested that a large proportion of mineralized DIC is fixed back into organic matter within the mat during the day, whereas it diffuses into the overlying brine at night.

In the gypsum and halite ponds, $\delta^{13}C_{DIC}$ gradually increased to reach 7.2‰ in CU-5. This increase indicates that the biological processes that reduced the $\delta^{13}C_{DIC}$ of the carbonate and gypsum ponds are suppressed in the halite ponds, and that $\delta^{13}C_{DIC}$ is primarily controlled by the degassing of CO_2(aq) (Stiller et al., 1985). A reduced influence of biological activity on $\delta^{13}C_{DIC}$ is consistent with the discussion about the $\delta^{13}C$ of pigments indicating that photosynthesis is more active in the lower salinity ponds.

Another observation is that DIC concentrations and TA in CH-1 and CU-5 were higher than those found in the solar saltern of Eilat, Israel (Lazar and Erez, 1992). These higher concentrations might be because the biological processes that potentially accumulate DIC and TA were more intense in the upper-stream, lower salinity ponds of the Trapani solar salterns. Indeed, as in CU-5, DIC and TA in the upstream ponds (CU-1 and CU-2) were

also slightly higher than the values reported by Lazar and Erez (1992), suggesting that biological processes in the lower salinity ponds accumulated in and modified the chemical composition of higher salinity ponds. Alternatively, the higher DIC and TA in the Trapani ponds may be due to dissolution of calcium carbonate supplied by aerial transport, because experimentally evaporated seawater is known to be undersaturated with respect to aragonite (Lazar et al., 1983).

Finally, the characteristic variation in *p*H is commonly observed in evaporating seawater brine (Bąbel and Schreiber, 2014), and it has been confirmed that this pattern is not an artifact from a liquid junction error in the glass *p*H electrode in the concentrated solution (Sass and Ben-Yaakov, 1977). In experimentally evaporated seawater, there is a continuous decrease in *p*H from seawater to the point where DE_{Mg} is around 6.7 (e.g., Lazar et al., 1983). Sass and Ben-Yaakov (1977) investigated the cause of such decrease in *p*H along the salinity gradient, and revealed that the apparent first and second dissociation constants of carbonic acid (K_1' and K_2') in the Dead Sea brine were about ten and thoudsand times larger than in seawater. They explained that the amount of CO_3^{2-} complexing with Mg^{2+} increases along the salinity gradient due to accumulation of Mg, which results in substantially large K_2' associating the *p*H lowering.

Thus, in the carbonate and gypsum ponds where benthic microbial mat is present, a decrease in *p*H as a result of $MgCO_3$ complexing was probably cancelled out by CO_2(aq) uptake for photosynthesis, which acts to increase *p*H. In the halite ponds, degassing of CO_2(aq) indicated from substantial increase in $\delta^{13}C_{DIC}$ should have lowered K_1' and K_2'. However, with reduced primary production comsuming CO_2(aq), the effect of $MgCO_3$ complexing dominated to lower the *p*H in the halite ponds.

II-5. Conclusions

In this chapter, I demonstrated that the isotopic fractionation factor (ε) calculated from $\delta^{13}C$ of chlorophyll *a* and β-carotene, which originate from cyanobacteria and algae, increased linearly along an increasing salinity gradient in solar saltern ponds in Trapani, Italy. This observation was ascribed to suppression of primary production with increasing salinity, and/or DIC-limited conditions within the microbial mats and gypsum crusts caused by restricted DIC diffusion from the overlying brine. Variations in the carbonate system parameters also indicate changing microbial activity along the salinity gradient. I propose that dissolution of atmospheric CO_2 into the brine through intensive CO_2(aq) uptake by photosynthesis and mineralization of organic matter by sulfate reduction may be the processes responsible for ^{13}C-depleted DIC in the carbonate and gypsum ponds. In contrast, increase in $\delta^{13}C_{DIC}$ in subsequent ponds was attributed to the dominance of degassing of CO_2(aq) with reduced microbial activity.

One important reason for elucidating the carbon cycle of hypersaline environments is that such environments may have had a substantial impact on the global carbon cycle during massive evaporation events that repeatedly occurred worldwide in the geological past (Hay et al., 2006; Warren, 2010). This chapter and previous studies (Stiller et al., 1985; Lazar and Erez, 1992) have demonstrated that CO_2 exchange between brine and the atmosphere is an important factor controlling the brine carbonate system during evaporation of seawater. Further investigations into the behavior of the carbonate system under various evaporative settings will enhance our understanding of the role of hypersaline environments in global carbon cycle.

Table II-1. Concentration of dissolved inorganic carbon (DIC) and its carbon isotopic composition ($\delta^{13}C_{DIC}$), total alkalinity (TA), and *p*H of seawater and brine from the Culcasi (CU), Sosalt (SS), and Chiusicella (CH) solar salterns in Trapani, Sicily, Italy. Numbers in the sample names refer to individual ponds at the salterns. SWS, seawater pH scale.

Sample	Type of evaporite	DIC (mmol L^{-1})	TA (mmol L^{-1})	$\delta^{13}C_{DIC}$ (‰)	pH (SWS)
CU-0	Seawater	2.04	2.68	2.2	8.2
CU-1	Carbonate	1.25	3.40	–5.0	8.5
CU-2	Carbonate	1.25	4.03	–10.6	8.5
SS-3	Carbonate	1.00	3.85	–8.6	8.3
SS-1	Gypsum	1.09	4.22	–8.2	8.2
SS-2	Gypsum	1.31	4.73	–9.9	8.0
CH-1	Gypsum	4.38	11.90	–3.2	7.5
SS-4	Halite	3.06	9.24	–5.2	7.3
CU-5	Halite	5.95	21.10	7.2	7.0

Table II-2. Salinity and concentrations of inorganic elements in seawater and brine from the solar salterns at Trapani, Sicily, Italy. CU, SS, and CH in the sample names refer to Culcasi, Sosalt, and Chiusicella salterns, respectively. Numbers in the sample names refer to specific ponds.

Sample	Type of evaporite	Salinity	Na^+ (mol L^{-1})	Mg^{2+} (mmol L^{-1})	K^+ (mmol L^{-1})	Ca^{2+} (mmol L^{-1})	Cl^- (mol L^{-1})	SO_4^{2-} (mmol L^{-1})	Br^- (mmol L^{-1})	B (mmol L^{-1})
CU-0	Seawater	38.2	0.52	57	11	12	0.60	31	0.90	0.57
CU-1	Carbonate	96.8	1.32	152	28	26	1.51	79	2.45	1.56
CU-2	Carbonate	126	1.69	196	36	33	1.95	101	2.87	1.98
SS-3	Carbonate	151	2.00	269	49	31	2.34	121	3.77	2.41
SS-1	Gypsum	159.1	2.09	282	51	31	2.46	126	4.21	2.75
SS-2	Gypsum	179.6	2.35	330	59	25	2.79	136	4.63	2.93
CH-1	Gypsum	-	-	678	119	9	-	233	8.47	5.55
SS-4	Halite	-	-	638	107	6	-	213	8.53	5.26
CU-5	Halite	-	-	1255	219	3	-	430	19.18	11.17

Table II-3. Descriptions of deposit samples and the carbon isotopic composition of their total organic carbon ($\delta^{13}C_{TOC}$). CU, SS, and CH in the sample names refer to the Culcasi, Sosalt, and Chiusicella salterns, respectively. Numbers in the sample names refer to specific ponds.

Sample		Type of evaporite	Description	$\delta^{13}C_{TOC}$ (‰)	Error (2σ)
CU-1	CU-1-1	Carbonate	Top slimy layer	–12.5	0.25
	CU-1-2		Bottom black layer	–8.6	0.25
CU-2	CU-2-1	Carbonate	Top slimy layer	–14.1	0.10
	CU-2-2		Bottom black layer	–13.8	0.10
SS-3	SS-3-1	Carbonate	Top slimy layer	–12.9	0.10
	SS-3-2		Bottom black layer	–14.2	0.10
SS-1	SS-1-1	Gypsum	Transparent layer	–13.2	0.25
	SS-1-2		Green layer	–16.2	0.25
	SS-1-3		Pink layer	–13.8	0.25
	SS-1-4		Black layer	–17.3	0.25
SS-2	SS-2-1	Gypsum	Transparent layer	–14.5	0.10
	SS-2-2		Green layer	–13.6	0.25
	SS-2-3		Pink layer	–15.7	0.25
	SS-2-4		Black layer	–15.1	0.25
CH-1	CH-1-1	Gypsum	Transparent layer	–16.0	0.25
	CH-1-2		Green layer	–15.7	0.25
	CH-1-3		Pink layer	–18.6	0.25
	CH-1-4		Black layer	–16.5	0.25
SS-4	SS-4	Halite	Halite crystal	–21.9	0.10
CU-5	CU-5	Halite	Halite crystal	–22.7	0.10

Table II-4. $\delta^{13}C$ of chlorophyll *a* (Chl *a*), bacteriochlorophyll *a* (BChl *a*), and β-carotene extracted from deposits collected from the Culcasi (CU), Sosalt (SS), and Chiusicella (CH) solar salterns in Trapani, Sicily, Italy. Numbers in the sample names refer to individual ponds at the salterns. Analytical errors are based on replicate measurements of standard material.

Sample	Type of evaporite	Layer	Compound	$\delta^{13}C$ (‰)	Error (2σ)
CU-1-1	Carbonate	Top slimy	Chl *a*	–11.5	0.23
			BChl *a*	–19.7	0.23
			β-carotene	–22.1	0.39
SS-3-1			Chl *a*	–20.1	0.15
			BChl *a*	–23.4	0.15
			β-carotene	–23.7	0.39
SS-1-1	Gypsum	Yellowish	Chl *a*	–17.9	0.23
			β-carotene	–25.9	0.37
SS-1-2		Green	Chl *a*	–17.0	0.23
SS-1-3		Pink	BChl *a*	–20.6	0.23
CH-1-1		Yellowish	Chl *a*	–20.6	0.15
			β-carotene	–23.6	0.57
CH-1-2		Green	Chl *a*	–18.6	0.23
CH-1-3		Pink	BChl *a*	–26.3	0.23
SS-4	Halite	Bulk crystal	β-carotene	–25.8	0.15
CU-5			β-carotene	–28.5	0.37

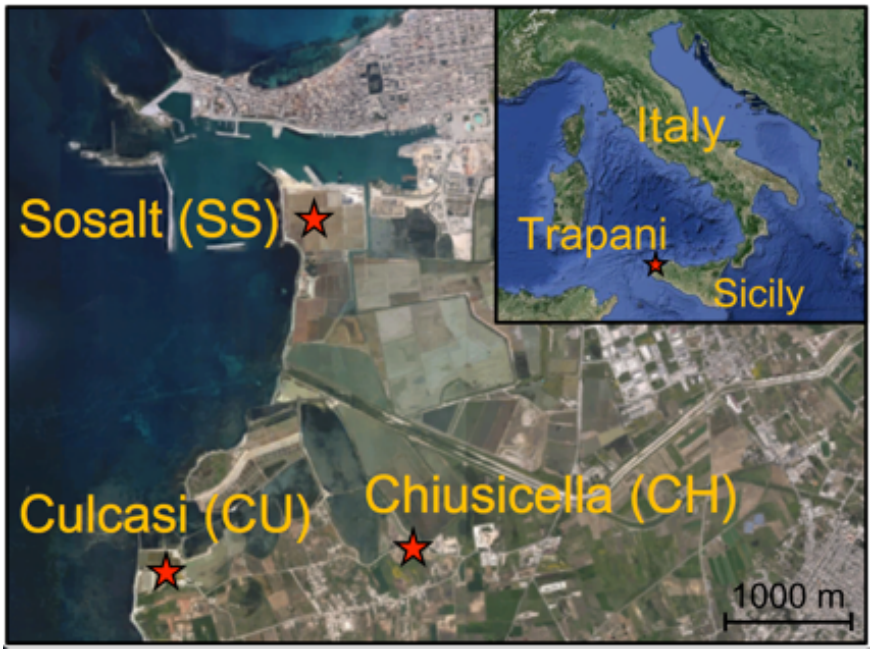

Fig. II-1. Locations of the solar salterns investigated in this chapter and Chapter III. The aerial image is from Google Earth.

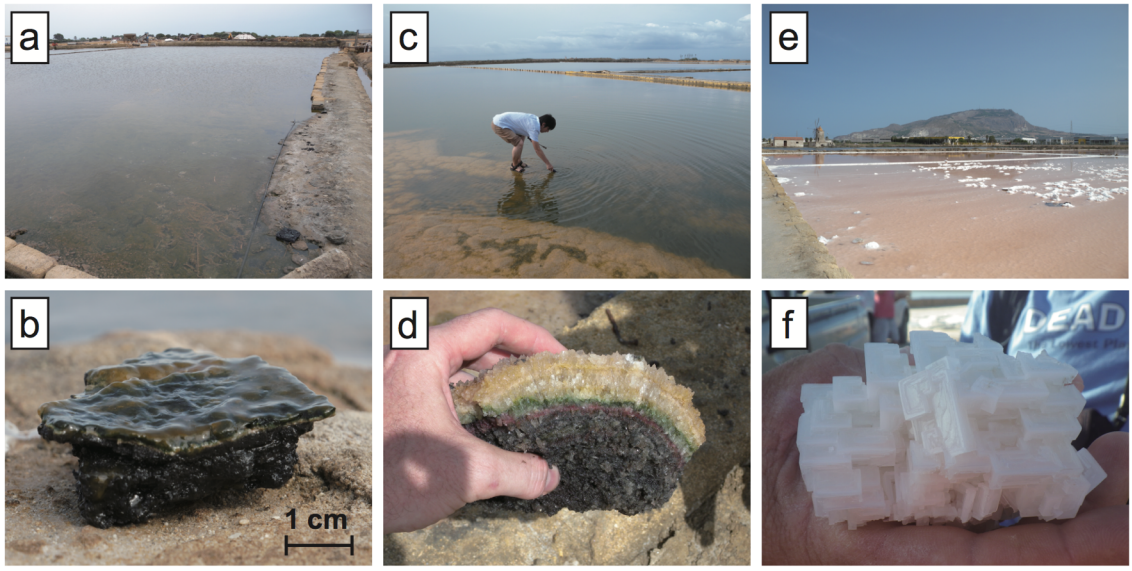

Fig. II-2. Photographs showing the appearance of the ponds and the bottom deposits. (a) carbonate pond; (b) bottom deposit of carbonate pond showing a slimy layer a few millimeters thick, which is composed of thin yellow, green, and pink layers on the surface, and black, loose deposits buried underneath; (c) gypsum pond; (d) gypsum crust from gypsum pond showing yellowish transparent, green, and pink layers, from the surface, and loose black deposits below; (e) halite pond; (f) halite crystals from halite pond.

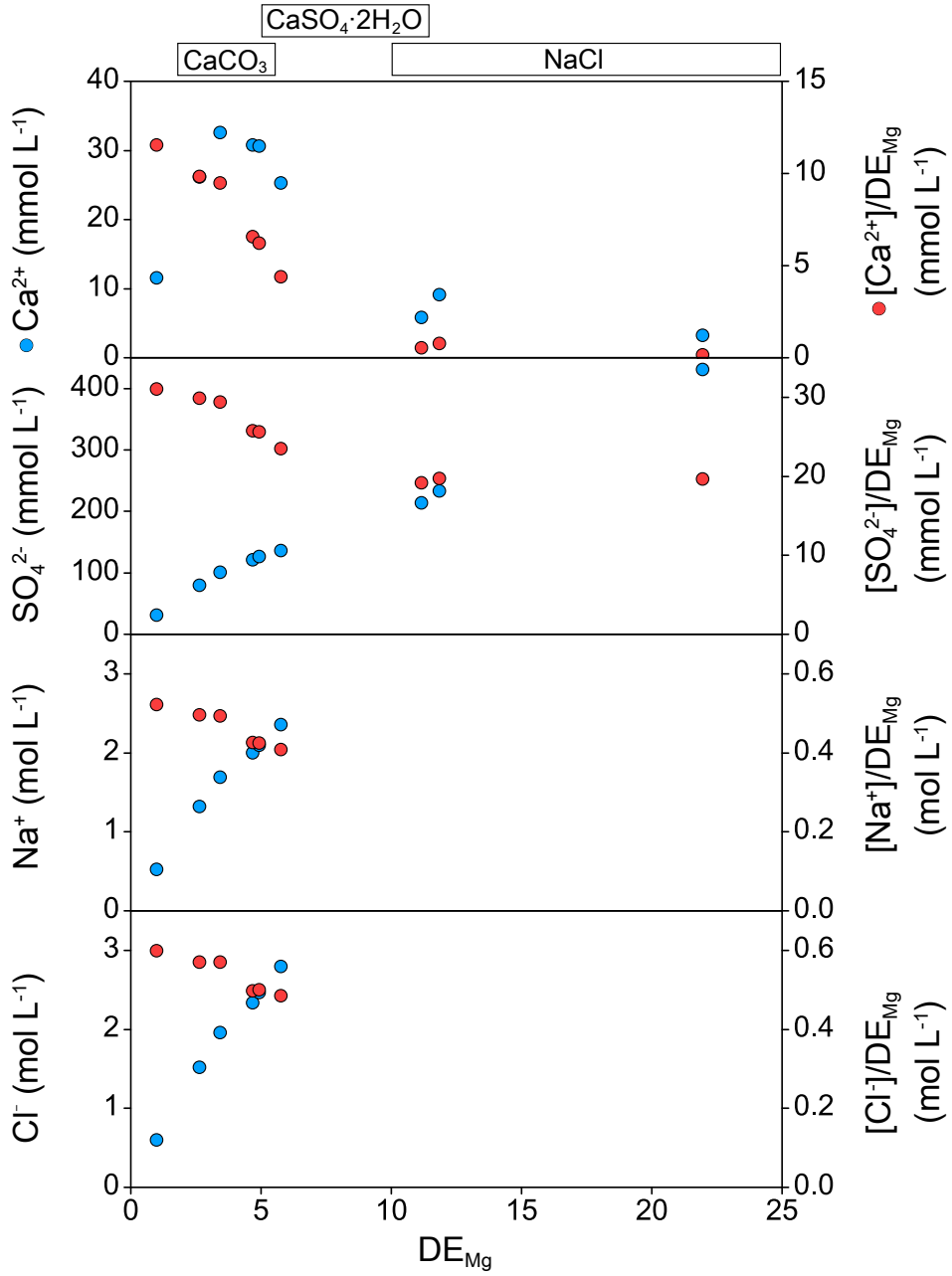

Fig. II-3. Variations in the concentrations of major ions (blue circles) and those normalized to the degree of evaporation as calculated from concentrations of magnesium ions (DE_{Mg}; red circles). The bars at the top of the figure show the precipitation ranges for calcium carbonate, gypsum, and halite.

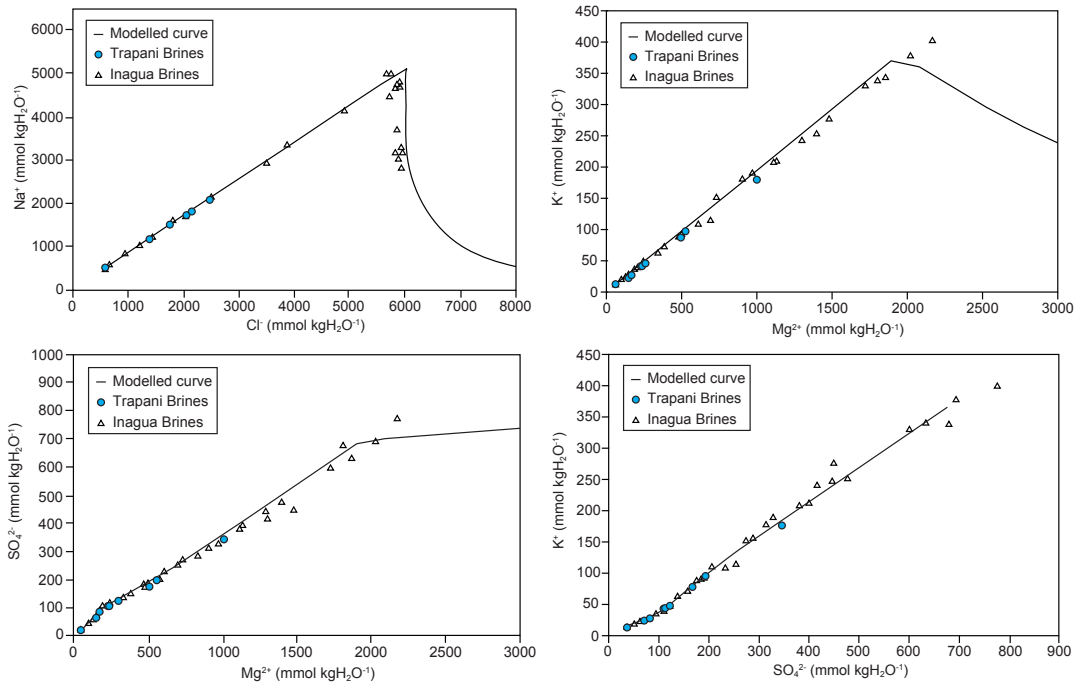

Fig. II-4. Cross plots of the major ions of the Trapani brines (blue circles) along with the computer-modeled evaporation path of modern seawater (solid lines: Timofeeff et al., 2001). Plotted for comparison are brine data from the Inagua crystallizer ponds (Bahamas) analyzed by McCaffrey et al. (1987) (blank triangles).

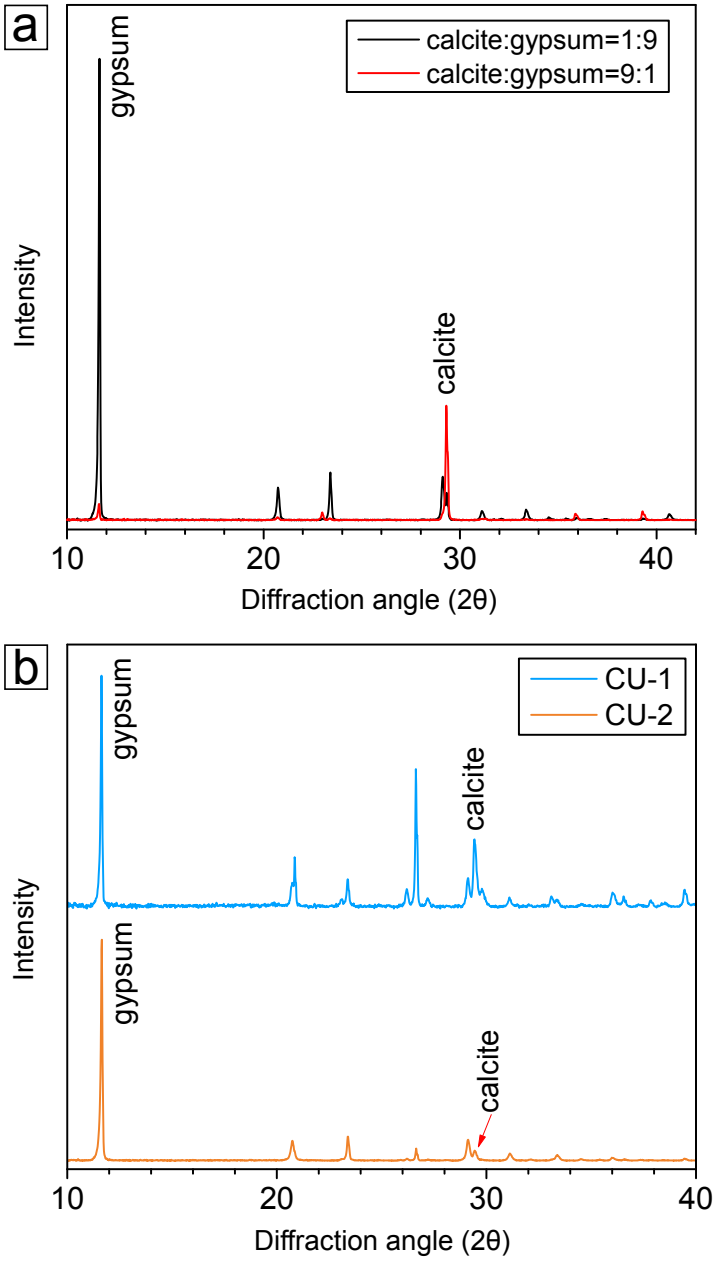

Fig. II-5 (a) The XRD patterns of mix standards consisting of calcite/[calcite+gypsum] = 0.1 in black line, and calcite/[calcite+gypsum] = 0.9 in red line. The height of the peaks at 2θ = 29.32 of calcite and 2θ = 11.64 of gypsum were used to draw the calibration curve. (b) The XRD patterns of the deposits of CU-1 (blue line) and CU-2 (orange line).

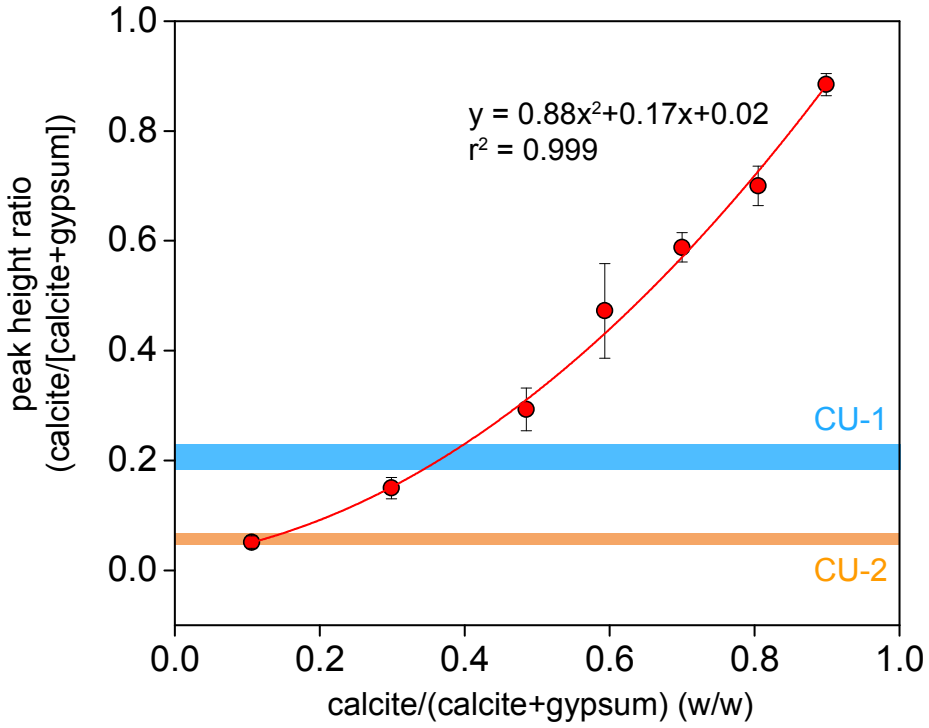

Fig. II-6 The relationship between the proportion of calcite relative to gypsum in the mix standard and the peak height ratio of calcite and gypsum. Average peak height ratios of the mix standards are depicted in red circle with the error bar (± 1σ), and the second order polynomial approximation line in red. Average peak height ratio of CU-1 and CU-2 are shown in blue and orange lines, respectively. The thickness of these lines represents their standard deviations (± 1σ).

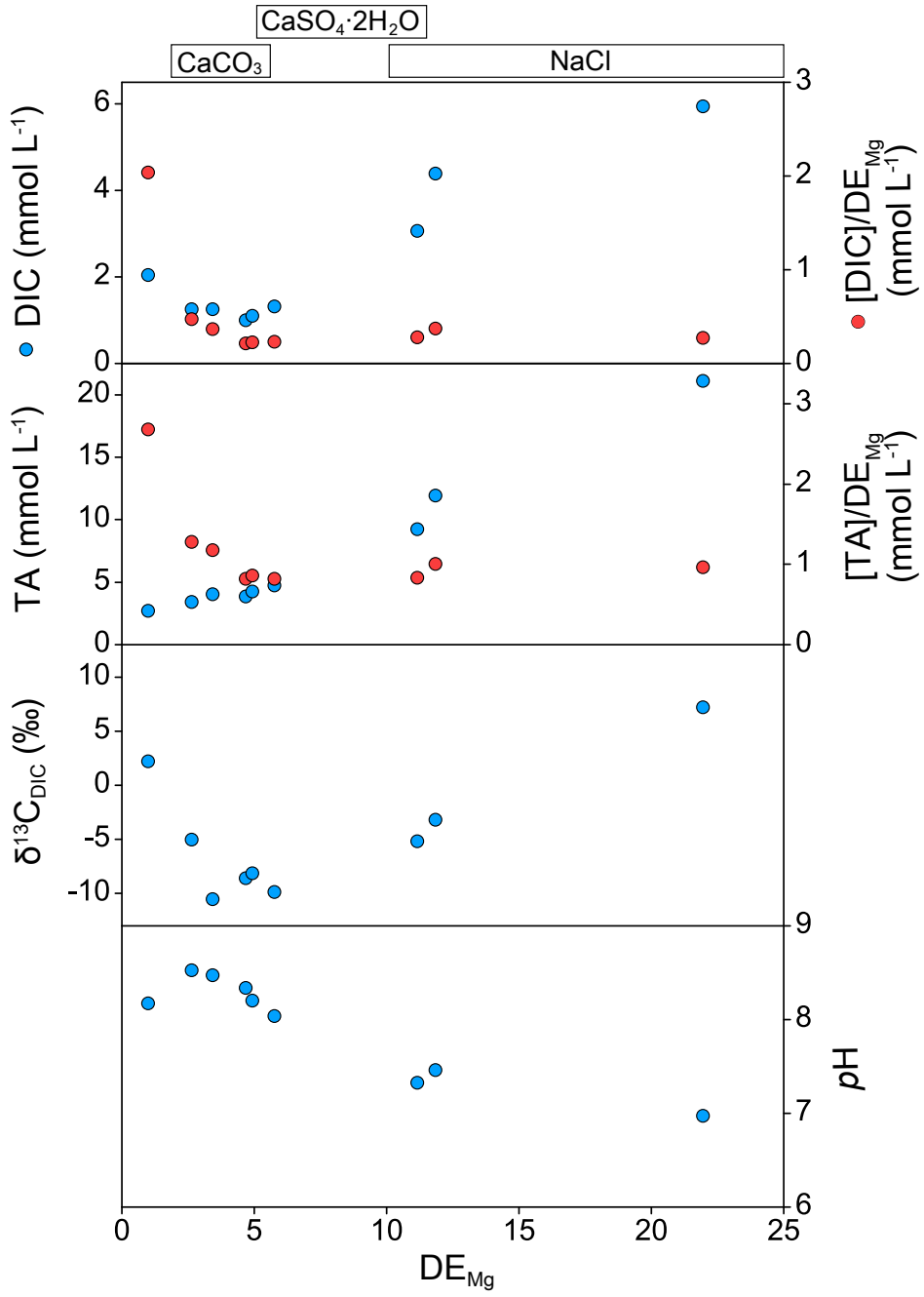

Fig. II-7. Variations in dissolved inorganic carbon (DIC) concentrations, total alkalinity (TA), $\delta^{13}C_{DIC}$, and *p*H (blue circles), and DIC and TA normalized to the degree of evaporation calculated from magnesium concentrations (DE_{Mg}; red circles). The bars at the top of the figure show the precipitation ranges for calcium carbonate, gypsum, and halite.

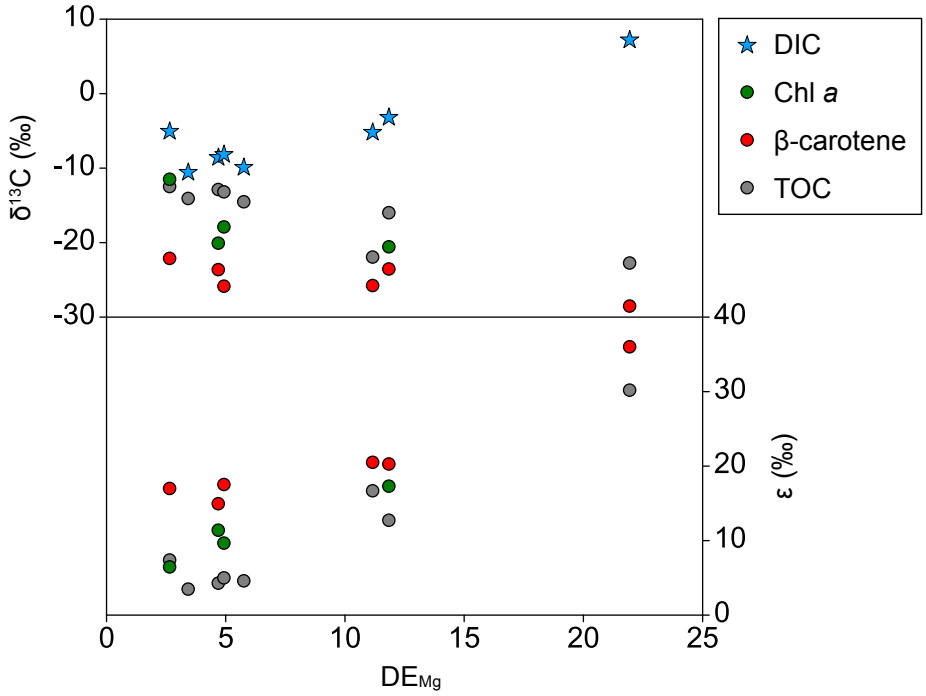

Fig. II-8. Variations in $\delta^{13}C$ of dissolved inorganic carbon (DIC, blue stars), total organic carbon (TOC, gray circles), chlorophyll *a* (green circles), and β-carotene (red circles), as well as the fractionation factor ε calculated from $\delta^{13}C$ of TOC and pigments.

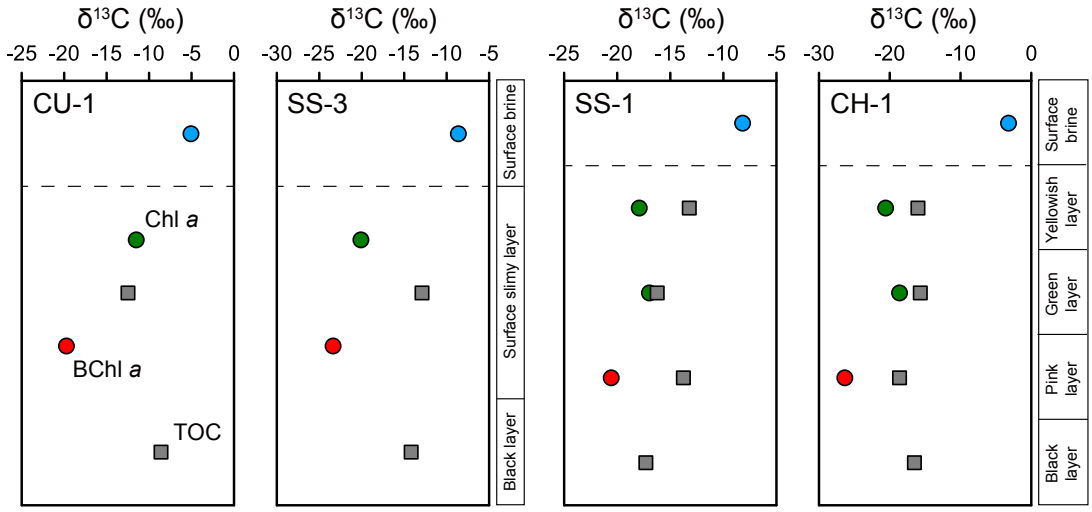

Fig. II-9. Depth profiles of $\delta^{13}C$ of chlorophyll *a* (Chl *a*) originating from cyanobacteria (green circles), bacteriochlorophyll *a* (BChl *a*) from purple sulfur bacteria (red circles), and total organic carbon (TOC, gray squares) in the microbial mats of the carbonate ponds (CU-1 and SS-3) and the gypsum crusts of the gypsum ponds (SS-1 and CH-1). Blue circles indicate the $\delta^{13}C$ of dissolved inorganic carbon (DIC) in the surface brine. CU, Culcasi; SS, Sosalt; CH, Chiusicella

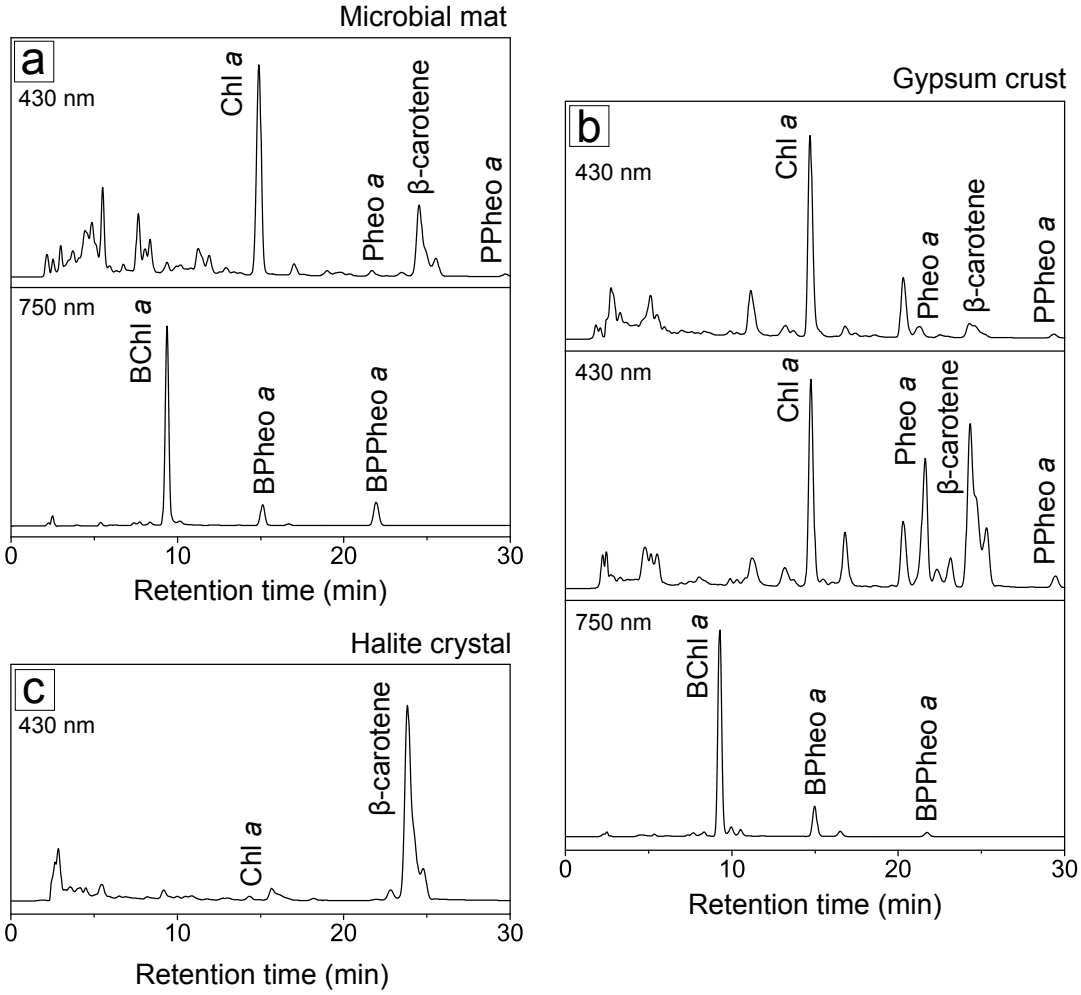

Fig. II-10 HPLC chromatograms of (a) the surface slimy layer of the microbial mat in a carbonate pond (monitored at 430 and 750 nm), (b) the yellowish transparent layer (430 nm), the green layer (430 nm), and the pink layer (750 nm) from the top of a gypsum crust, and (c) halite (430 nm). Chl *a*, chlorophyll *a*; BChl *a*, bacteriochlorophyll *a*; Pheo *a*, pheophytin *a*; BPheo *a*, bacteriopheophytin *a*; PPheo *a*, pyropheophytin *a*; BPPheo *a*, bacteriopyropheophytin *a*.

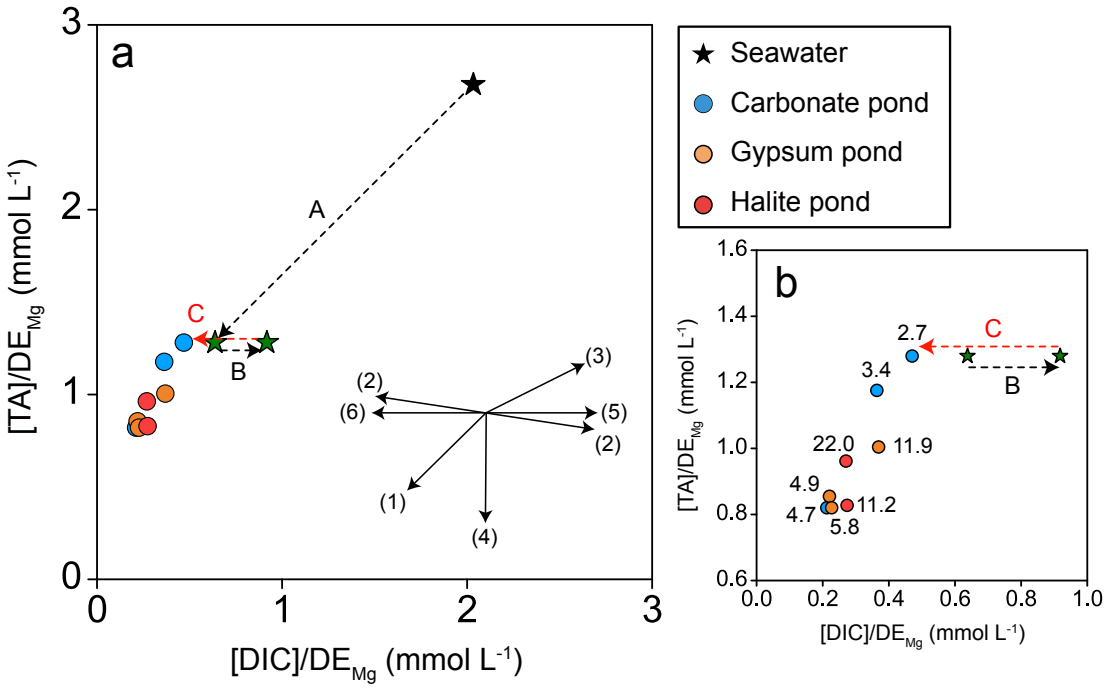

Fig. II-11. (a) Cross plot of dissolved inorganic carbon (DIC) concentrations and total alkalinity (TA) normalized to the degree of evaporation based on magnesium ion concentrations ([DIC]/DE_{Mg} and [TA]/DE_{Mg}, respectively). Dotted black arrows A and B indicate changes due to utilization of HCO_3^- and re-dissolution of CO_2(g) by calcium carbonate precipitation during the transition from seawater (CU-0) to the carbonate pond (CU-1, DE_{Mg} = 2.7), respectively. Dotted red arrow C indicates the supply of DIC necessary to explain [DIC]/DE_{Mg} and [TA]/DE_{Mg} in CU-1. Solid arrows in the bottom right corner indicate the direction and slope of the following processes: (1) calcium carbonate precipitation, (2) photosynthesis and respiration, (3) sulfate reduction, (4) sulfide oxidation, (5) dissolution of atmospheric CO_2, and (6) degassing of CO_2(aq). (b) Close-up view of (a). Numbers next to the symbols are DE_{Mg} values. CU, Culcasi.

CHAPTER III

THE NITROGEN CYCLE IN THE MODERN SHALLOW HYPERSALINE ENVIRONMENTS

本章については、5 年以内に雑誌等で刊行予定のため、非公開。

CHAPTER IV

BIOLOGICAL AND ENVIRONMNENTAL CHANGES DURING THE INITIAL STAGE OF THE MESSINIAN SALINITY CRISIS

本章については、5 年以内に雑誌等で刊行予定のため、非公開。

CHAPTER V

BIOLOGICAL AND ENVIRONMNENTAL CONDITIONS DURING THE PEAK OF THE MESSINIAN SALINITY CRISIS

本章については、5 年以内に雑誌等で刊行予定のため、非公開。

CHAPTER VI

GENERAL SUMMARY AND IMPLICATIONS

本章については、5 年以内に雑誌等で刊行予定のため、非公開。

References

Airs, R.L., and Keely, B.J. (2003) A high resolution study of the chlorophyll and bacteriochlorophyll pigment distributions in a calcite/gypsum microbial mat. *Org. Geochem.* **34**, 539–551.

Altabet, M.A. and Francois, R. (1994) Sedimentary nitrogen isotopic ratio as a recorder for surface ocean nitrate utilization. *Global Biogeochem. Cycles* **8**, 103–116.

Altabet, M.A., Pilskaln, C., Thunell, R., Pride, C., Sigman, D., Chavez, F. and Francois, R. (1999) The nitrogen isotope biogeochemistry of sinking particles from the margin of the Eastern North Pacific. *Deep Sea Res. Part I Oceanogr. Res. Pap.* **46**, 655–679.

Antón J., Rosselló-Mora R., Rodríguez-Valera F., and Amann R. (2000) Extremely halophilic bacteria in crystallizer ponds from solar saltern. *Appl. Environ. Microbiol.* **66**, 3052–3057.

Arnaboldi, M. and Meyers, P.A. (2006) Patterns of organic carbon and nitrogen isotopic compositions of latest Pliocene sapropels from six locations across the Mediterranean Sea. *Palaeogeogr., Palaeoclimatol., Palaeoecol.* **235**, 149–167.

Babel M., and Schreiber B.C. (2014) Geochemistry of evaporites and evolution of seawater. In *Treatise on geochemistry, 2nd edn.* (eds. Holland, H. and Turekian, K.). Elsevier, Oxford. pp. 483–560.

Badger, M.P., Lear, C.H., Pancost, R.D., Foster, G.L., Bailey, T.R., Leng, M.J. and Abels, H.A. (2013) CO_2 drawdown following the middle Miocene expansion of the Antarctic Ice Sheet. *Paleoceanography* **28**, 42–53.

Badger M.R., and Price G.D. (2003) CO_2 concentrating mechanisms in cyanobacteria: molecular components, their diversity and evolution. *J. Exp. Bot.* **54**, 609–622.

Baertschi P. (1952) Die Fraktionierung der Kohlenstoffisotopen bei der absorption von Kohlendioxyd. *Helv. Chim. Acta* **35**, 1030–1036.

Baker, E.W. and Louda, J.W. (1986) Porphyrins in the geological record. In *Biological Markers in Sediments. Methods in Geochemistry and Geophysics, vol. 24.* (eds. Johns, R.B.) Elsevier, Amsterdam, pp. 125–225.

Barford, C.C., Montoya, J.P., Altabet, M.A. and Mitchell, R. (1999) Steady-state nitrogen isotope effects of N_2 and N_2O production in *Paracoccus denitrificans*. *Appl. Environ. Microbiol.* **65**, 989–994.

Barkan E., Luz B., and Lazar B. (2001) Dynamics of the carbon dioxide system in the Dead Sea. *Geochim. Cosmochim. Acta* **65**, 355–368.

Baumgartner L.K., Reid R.P., Dupraz C., Decho A.W., Buckley D.H., Spear J.R., Przekop K.M., and Visscher P.T. (2006) Sulfate reducing bacteria in microbial mats: changing paradigms, new discoveries. *Sediment. Geol.* **185**, 131–145.

Beale, S.I., Gough, S.P., and Granick, S. (1975) Biosynthesis of δ-aminolevulinic acid from the intact carbon skeleton of glutamic acid in greening barley. *Proc. Natl. Acad. Sci. U.S.A.* **72**, 2719–2723.

Beaumont, V.I., Jahnke, L.L., and Des Marais, D.J. (2000) Nitrogen isotopic fractionation in the synthesis of photosynthetic pigments in *Rhodobacter capsulatus* and *Anabaena cylindrica*. *Org. Geochem.* **31**, 1075–1085.

Bebout, B.M., Paerl, H.W., Bauer, J.E., Canfield, D.E., amd Des Marais, D.J. (1994) Nitrogen cycling in microbial mat communities: The quantitative importance of N-fixation and other sources of N for primary productivity. In *Microbial Mats: Structure, Development and Environmental Significance*, (eds. Stal, L.J., and Caumette, P.) Springer-Verlag, Berlin, NATO ASI Series, vol. 35, pp. 265–271.

Benlloch, S., López-López, A., Casamayor, E.O., Øvreås, L., Goddard, V., Daae, F.L., Smerdon, G., Massana, R., Joint, I. and Thingstad, F. (2002) Prokaryotic genetic diversity throughout the salinity gradient of a coastal solar saltern. *Environ. Microbiol.* **4**, 349–360.

Bergé, J.P. and Barnathan, G. (2005) Fatty acids from lipids of marine organisms: molecular biodiversity, roles as biomarkers, biologically active compounds, and economical aspects. In *Marine biotechnology I. Advances in Biochemical Engineering/Biotechnology*. (eds. Ulber, R. and Le Gal, Y.) Springer, Springer, Berlin, Heidelberg, Vol. 96, pp. 49–125.

Berger, W.H., Smetacek, V.S., and Wefer, G. (1989) *Productivity of the Ocean: Present and Past*. Wiley-Interscience, New York, pp. 470.

Berman-Frank, I., Bidle, K.D., Haramaty, L. and Falkowski, P.G. (2004) The demise of the marine cyanobacterium, *Trichodesmium spp.*, via an autocatalyzed cell death pathway. *Limnol. Oceanogr.* **49**, 997–1005.

Bertini, A. (2006) The Northern Apennines palynological record as a contribute for the reconstruction of the Messinian palaeoenvironments. *Sediment. Geol.* **188**, 235–258.

Bertini, A., Londeix, L., Maniscalco, R., Di Stefano, A., Suc, J.P., Clauzon, G., Gautier, F. and Grasso, M. (1998) Paleobiological evidence of depositional conditions in the Salt Member, Gessoso-Solfifera Formation (Messinian, Upper Miocene) of Sicily. *Micropaleontology* **44**, 413–433.

Bidigare, R.R., Fluegge, A., Freeman, K.H., Hanson, K.L., Hayes, J.M., Hollander, D., Jasper, J.P., King, L.L., Laws, E.A. and Milder, J. (1997) Consistent fractionation of ^{13}C in nature and in the laboratory: Growth-rate effects in some haptophyte algae. *Global Biogeochem. Cycles* **11**, 279–292.

Bidigare R.R., Hanson K.L., Buessler K.O., Wakeham S.G., Freeman K.H., Pancost R.D., Millero F.J., Steinberg P., Popp B.N., Latasa M., Landry M.R., and Laws E.A. (1999)

Iron-stimulated changes in ^{13}C fractionation and export by equatorial Pacific phytoplankton: toward a paleogrowth rate proxy. *Paleoceanography* **14**, 589–595.

Blanc-Valleron, M.M., Pierre, C., Caulet, J., Caruso, A., Rouchy, J.M., Cespuglio, G., Sprovieri, R., Pestrea, S. and Di Stefano, E. (2002) Sedimentary, stable isotope and micropaleontological records of paleoceanographic change in the Messinian Tripoli Formation (Sicily, Italy). *Palaeogeogr., Palaeoclimatol., Palaeoecol.* **185**, 255–286.

Boreham, C.J., Fookes, C.J., Popp, B.N. and Hayes, J. (1989) Origins of etioporphyrins in sediments: evidence from stable carbon isotopes. *Geochim. Cosmochim. Acta* **53**, 2451–2455.

Boreham, C.J., Fookes, C.J., Popp, B.N. and Hayes, J. (1990) Origin of petroporphyrins. 2. Evidence from stable carbon isotopes. *Energy Fuels* **4**, 658–661.

Borin, S., Mapelli, F., Rolli, E., Song, B., Tobias, C., Schmid, M.C., De Lange, G.J., Reichart, G.J., Schouten, S. and Jetten, M. (2013) Anammox bacterial populations in deep marine hypersaline gradient systems. *Extremophiles* **17**, 289–299.

Boyle, E.A. (1988) Vertical oceanic nutrient fractionation and glacial/interglacial CO_2 cycles. *Nature* **331**, 55–56.

Brandes, J.A., Devol, A.H. and Deutsch, C. (2007) New developments in the marine nitrogen cycle. *Chem. Rev.* **107**, 577–589.

Brandes, J.A., Devol, A.H., Yoshinari, T., Jayakumar, D. and Naqvi, S. (1998) Isotopic composition of nitrate in the central Arabian Sea and eastern tropical North Pacific: A tracer for mixing and nitrogen cycles. *Limnol. Oceanogr.* **43**, 1680–1689.

Brown, A. (1990) *Microbial water stress physiology. Principles and perspectives.* Wiley, Chichester, U.K.

Callot, H.J., Ocampo, R. (2000) Geochemistry of porphyrins. In *The Porphyrin Handbook, Synthetic and Organic Chemistry, vol. 1.* (eds. Kadish, K.M., Smith, K.M., and Guiland, R.) Academic Press, New York, pp. 349–398.

Calvert, S., Nielsen, B. and Fontugne, M. (1992) Evidence from nitrogen isotope ratios for enhanced productivity during formation of eastern Mediterranean sapropels. *Nature* **359**, 223–225.

Canfield, D.E. and Des Marais, D.J. (1991) Aerobic sulfate reduction in microbial mats. *Science* **251**, 1471–1473.

Canfield D.E., and Des Marais D.J. (1993) Biogeochemical cycles of carbon, sulfur, and free oxygen in a microbial mat. *Geochim. Cosmochim. Acta* **57**, 3971–3984.

Canfield D.E., Sørensen K.B., and Oren A. (2004) Biogeochemistry of a gypsum-encrusted microbial ecosystem. *Geobiology* **2**, 133–150.

Capone, D.G., Bronk, D.A., Mulholland, M.R. and Carpenter, E.J. (2008) *Nitrogen in the marine environment.* Academic Press, Yew York.

Capone, D.G., Zehr, J.P., Paerl, H.W., Bergman, B. and Carpenter, E.J. (1997) *Trichodesmium*, a globally significant marine cyanobacterium. *Science* **276**, 1221–1229.

Carnevale, G., Longinelli, A., Caputo, D., Barbieri, M. and Landini, W. (2008) Did the Mediterranean marine reflooding precede the Mio–Pliocene boundary? Paleontological and geochemical evidence from upper Messinian sequences of Tuscany, Italy. *Palaeogeogr., Palaeoclimatol. Palaeoecol.* **257**, 81–105.

Carpenter, E.J., Montoya, J.P., Burns, J., Mulholland, M.R., Subramaniam, A. and Capone, D.G. (1999) Extensive bloom of a N_2-fixing diatom/cyanobacterial association in the tropical Atlantic Ocean. *Mar. Ecol. Prog. Ser.* **185**, 273–283.

Casciotti, K.L. (2016) Nitrogen and oxygen isotopic studies of the marine nitrogen cycle. *Ann. Rev. Mar. Sci.* **8**, 379–407.

Casciotti, K.L., Sigman, D.M., Hastings, M.G., Böhlke, J. and Hilkert, A. (2002) Measurement of the oxygen isotopic composition of nitrate in seawater and freshwater using the denitrifier method. *Anal. Chem.* **74**, 4905–4912.

Caumette, P., Matheron, R., Raymond, N. and Relexans, J.C. (1994) Microbial mats in the hypersaline ponds of Mediterranean salterns (Salins-de-Giraud, France). *FEMS Microbiol. Ecol.* **13**, 273–286.

Cerling, T.E., Harris, J.M., MacFadden, B.J., Leakey, M.G., Quade, J., Eisenmann, V. and Ehleringer, J.R. (1997) Global vegetation change through the Miocene/Pliocene boundary. *Nature* **389**, 153–158.

Chan, Q.H., Zolensky, M.E., Kebukawa, Y., Fries, M., Ito, M., Steele, A., Rahman, Z., Nakato, A., Suga, H., Takahashi, Y., Takeichi, Y. and Mase, K. (2018) Organic matter in extraterrestrial water-bearing salt crystals. *Science Advances* **4**, eaao3521.

Chicarelli, M.I., Hayes, J., Popp, B.N., Eckardt, C.B. and Maxwell, J.R. (1993) Carbon and nitrogen isotopic compositions of alkyl porphyrins from the Triassic Serpiano oil shale. *Geochim. Cosmochim. Acta* **57**, 1307–1311.

Chikaraishi, Y., Kaneko, M. and Ohkouchi, N. (2012) Stable hydrogen and carbon isotopic compositions of long-chain (C_{21}–C_{33}) *n*-alkanes and *n*-alkenes in insects. *Geochim. Cosmochim. Acta* **95**, 53–62.

Chikaraishi, Y., Ogawa, N.O., Kashiyama, Y., Takano, Y., Suga, H., Tomitani, A., Miyashita, H., Kitazato, H. and Ohkouchi, N. (2009) Determination of aquatic food-web structure based on compound-specific nitrogen isotopic composition of amino acids. *Limnol. Oceanogr. Methods* **7**, 740–750.

Chillier, X.F.D., Gülaçar, F.O. and Buchs, A. (1993) A novel sedimentary lacustrine chlorin: characterisation and geochemical significance. *Chemosphere* **27**, 2103–2110.

CIESM (2008) The Messinian salinity crisis from mega-deposits to microbiology. In *A*

consensus report, in 33ème CIESM Workshop Monographs, vol. 33. (eds. Briand, F.) CIESM, Monaco, pp. 1–168.

Collister, J.W., and Hayes, J.M. (1991) A preliminary study of the carbon and nitrogen isotopic biogeochemistry of lacustrine sedimentary rocks from the Green River Formation, Wyoming, Utah, and Colorado. In *Geochemical, Biogeochemical, and Sedimentological Studies of the Green River Formation, Wyoming, Utah and Colorado*. (ed. Tuttle, M.) U.S. Geological Survey Bulletin, Washington, pp. C1–C16.

Dähnke, K., Moneta, A., Veuger, B., Soetaert, K. and Middelburg, J. (2012) Balance of assimilative and dissimilative nitrogen processes in a diatom-rich tidal flat sediment. *Biogeosciences* **9**, 4059.

De Lange, G.J. and Krijgsman, W. (2010) Messinian salinity crisis: A novel unifying shallow gypsum/deep dolomite formation mechanism. *Mar. Geol.* **275**, 273–277.

de Wit, R., I. Falcón, L. and Charpy-Roubaud, C. (2005) Heterotrophic dinitrogen fixation (acetylene reduction) in phosphate-fertilised *Microcoleus chthonoplastes* microbial mat from the hypersaline inland lake 'la Salada de Chiprana' (NE Spain). *Hydrobiologia* **534**, 245–253.

Decima, A. and Wezel, F. (1973) Late Miocene evaporites of the central Sicilian basin, Italy. *Initial Reports of the Deep Sea Drilling Project* **13**, 1234–1241.

Dela Pierre, F., Bernardi, E., Cavagna, S., Clari, P., Gennari, R., Irace, A., Lozar, F., Lugli, S., Manzi, V. and Natalicchio, M. (2011) The record of the Messinian salinity crisis in the Tertiary Piedmont Basin (NW Italy): the Alba section revisited. *Palaeogeogr. Palaeoclimatol. Palaeoecol.* **310**, 238–255.

Dela Pierre, F., Natalicchio, M., Ferrando, S., Giustetto, R., Birgel, D., Carnevale, G., Gier, S., Lozar, F., Marabello, D. and Peckmann, J. (2015) Are the large filamentous microfossils preserved in Messinian gypsum colorless sulfide-oxidizing bacteria? *Geology* **43**, 855–858.

Des Marais D.J. (2003) Biogeochemistry of hypersaline microbial mats illustrates the dynamics of modern microbial ecosystems and the early evolution of the biosphere. *Biol. Bull.* **204**, 160–167.

Des Marais D.J., and Canfield D.E. (1994) The carbon isotope biogeochemistry of microbial mats. In *Microbial Mats: Structure, Development and Environmental Significance* (eds. Stal L.J. and Caumette P.). Springer, Berlin. NATO ASI Series G, Vol. 35, pp. 289–298.

Deutsch, C., Sarmiento, J.L., Sigman, D.M., Gruber, N. and Dunne, J.P. (2007) Spatial coupling of nitrogen inputs and losses in the ocean. *Nature* **445**, 163–167.

Duggen, S., Hoernle, K., Van Den Bogaard, P., Rüpke, L. and Morgan, J.P. (2003) Deep roots of the Messinian salinity crisis. *Nature* **422**, 602–606.

Eglinton, G. and Hamilton, R.J. (1967) Leaf epicuticular waxes. *Science* **156**, 1322–1335.

Flecker, R., Krijgsman, W., Capella, W., de Castro Martíns, C., Dmitrieva, E., Mayser, J.P., Marzocchi, A., Modestou, S., Ochoa, D. and Simon, D. (2015) Evolution of the Late Miocene Mediterranean–Atlantic gateways and their impact on regional and global environmental change. *Earth Sci. Rev.* **150**, 365–392.

Fogel, M.L., and Cifuentes, L.A. (1993) Isotope fractionation during primary production. In *Organic Geochemistry: Principles and Applications* (eds. Engel, M. H., Macko, S. A.) Springer, New York, pp. 73–98.

Fontugne, M.R. and Calvert, S.E. (1992) Late Pleistocene variability of the carbon isotopic composition of organic matter in the eastern Mediterranean: Monitor of changes in carbon sources and atmospheric CO_2 concentrations. *Paleoceanography* **7**, 1–20.

Fookes, C.J. (1983) Identification of a homologous series of nickel (II) 15, 17-butanoporphyrins from an oil shale. *J. Chem. Soc., Chem. Commun.* **24,** 1474–1476.

Fortuin, A.R. and Krijgsman, W. (2003) The Messinian of the Nijar Basin (SE Spain): sedimentation, depositional environments and paleogeographic evolution. *Sediment. Geol.* **160**, 213–242.

Foster, R. and O'Mullan, G. (2008) Nitrogen-fixing and nitrifying symbioses in the marine environment. In *Nitrogen in the marine environment*. (eds. Capone, D.G., Bronk, D.A., Mulholland, M.R., and Carpenter, E.J.) Academic Press, New York, pp. 1197–1218.

Foster, R., Subramaniam, A., Mahaffey, C., Carpenter, E., Capone, D. and Zehr, J. (2007) Influence of the Amazon River plume on distributions of free-living and symbiotic cyanobacteria in the western tropical North Atlantic Ocean. *Limnol. Oceanogr.* **52**, 517–532.

Frankignoulle, M., Canon, C. and Gattuso, J.P. (1994) Marine calcification as a source of carbon dioxide: Positive feedback of increasing atmospheric CO_2. *Limnol. Oceanogr.* **39**, 458–462.

Freudenthal, T., Wagner, T., Wenzhöfer, F., Zabel, M. and Wefer, G. (2001) Early diagenesis of organic matter from sediments of the eastern subtropical Atlantic: evidence from stable nitrogen and carbon isotopes. *Geochim. Cosmochim. Acta* **65**, 1795–1808.

Friedman, G. M. and Sanders, J. E. (1978) Principles of sedimentology. Wiley.

Fründ, C. and Cohen, Y. (1992) Diurnal cycles of sulfate reduction under oxic conditions in cyanobacterial mats. *Appl. Environ. Microbiol.* **58**, 70-77.

Fulton, J.M., Arthur, M.A. and Freeman, K.H. (2012) Black Sea nitrogen cycling and the preservation of phytoplankton $\delta^{15}N$ signals during the Holocene. *Global Biogeochem.*

Cycles **26**, GB2030.

Garcia-Castellanos, D. and Villasenor, A. (2011) Messinian salinity crisis regulated by competing tectonics and erosion at the Gibraltar arc. *Nature* **480**, 359–363.

Garcia-Veigas, J., Orti, F., Rosell, L., Ayora, C., Rouchy, J.M. and Lugli, S. (1995) The Messinian salt of the Mediterranean: geochemical study of the salt from the Central Sicily Basin and comparison with the Lorca Basin (Spain). *Bull. Soc. Géol. France* **166**, 699–710.

Geisler-Cussey D. (1997) Modern depositional facies developed in evaporative environments (marine, mixed, and nonmarine). In *Sedimentary Deposition in Rift and Foreland Basins in France and Spain (Paleogene and Lower Neogene)* (eds. Busson G. and Schreiber B.C.). Columbia University Press, New York. pp. 3–42.

Goericke, R., Strom, S.L. and Bell, M.A. (2000) Distribution and sources of cyclic pheophorbides in the marine environment. *Limnol. Oceanogr.* **45**, 200–211.

Golan, R., Gavrieli, I., Ganor, J. and Lazar, B. (2016) Controls on the *p*H of hyper-saline lakes–A lesson from the Dead Sea. *Earth. Planet. Sci. Lett*. **434**, 289–297.

Green, S.J., Blackford, C., Bucki, P., Jahnke, L.L. and Prufert-Bebout, L. (2008) A salinity and sulfate manipulation of hypersaline microbial mats reveals stasis in the cyanobacterial community structure. *The ISME journal* **2**, 457–470.

Gruber N. (2004) The Dynamics of the Marine Nitrogen Cycle and its Influence on Atmospheric CO_2 Variations. In *The Ocean Carbon Cycle and Climate. NATO Science Series (Series IV: Earth and Environmental Sciences), vol 40.* (eds. Follows M. and Oguz T.) Springer, Dordrecht, pp. 97–148.

Gruber, N. (2008) The marine nitrogen cycle: overview and challenges. In *Nitrogen in the marine environment*. (eds. Capone, D.G., Bronk, D.A., Mulholland, M.R., and Carpenter, E.J.) Academic Press, New York, pp. 1–50.

Guerzoni, S., Chester, R., Dulac, F., Herut, B., Loÿe-Pilot, M.D., Measures, C., Migon, C., Molinaroli, E., Moulin, C. and Rossini, P. (1999) The role of atmospheric deposition in the biogeochemistry of the Mediterranean Sea. *Prog. Oceanogr.* **44**, 147–190.

Hallsworth, J.E., Yakimov, M.M., Golyshin, P.N., Gillion, J.L., D'Auria, G., de Lima Alves, F., La Cono, V., Genovese, M., McKew, B.A., Hayes, S.L., Harris, G., Giuliano, L., Timmis, K.N. and McGenity, T.J. (2007) Limits of life in $MgCl_2$-containing environments: chaotropicity defines the window. *Environ. Microbiol.* **9**, 801–813.

Hanschmann, G. (1981) Berechnung von Isotopieeffekten auf quantenchemischer Grundlage am Beispiel sticksoffhaltiger Molekule. *ZfI-Mitt.* **41**, 19–39.

Hardie, L.A. and Lowenstein, T.K. (2004) Did the Mediterranean Sea dry out during the Miocene? A reassessment of the evaporite evidence from DSDP Legs 13 and 42A cores. *J. Sed. Res.* **74**, 453-461.

Hardie, L.A., Lowenstein, T.K., and Spencer R.J. (1985) The problem of distinguishing between primary and secondary features in evaporites. In *6th International Symposium on Salt Vol. 1*. (ed. Schreiber, B.C.), Salt Institute, pp. 11–39.

Hay, W.W., Migdisov, A., Balukhovsky, A.N., Wold, C.N., Flögel, S. and Söding, E. (2006) Evaporites and the salinity of the ocean during the Phanerozoic: Implications for climate, ocean circulation and life. *Palaeogeogr. Palaeoclimatol. Palaeoecol.* **240**, 3–46.

Hayes, J., Takigiku, R., Ocampo, R., Callot, H. J. and Albrecht, P. (1987) Isotopic compositions and probable origins of organic molecules in the Eocene Messel shale. *Nature* **329**, 48–51.

Higgins, M.B., Robinson, R.S., Carter, S.J. and Pearson, A. (2010) Evidence from chlorin nitrogen isotopes for alternating nutrient regimes in the Eastern Mediterranean Sea. *Earth. Planet. Sci. Lett.* **290**, 102–107.

Higgins, M.B., Robinson, R.S., Husson, J.M., Carter, S.J. and Pearson, A. (2012) Dominant eukaryotic export production during ocean anoxic events reflects the importance of recycled NH_4^+. *Proc. Natl. Acad. Sci. U.S.A.* **109**, 2269–2274.

Higgins, M.B., Wolfe-Simon, F., Robinson, R.S., Qin, Y., Saito, M. A. and Pearson, A. (2011) Paleoenvironmental implications of taxonomic variation among $\delta^{15}N$ values of chloropigments. *Geochim. Cosmochim. Acta* 75, 7351–7363.

Hilgen, F., Krijgsman, W., Langereis, C., Lourens, L., Santarelli, A. and Zachariasse, W. (1995) Extending the astronomical (polarity) time scale into the Miocene. *Earth. Planet. Sci. Lett.* **136**, 495–510.

Hiscock, W.T. and Millero, F.J. (2006) Alkalinity of the anoxic waters in the Western Black Sea. *Deep Sea Res. Part II Top. Stud. Oceanogr.* **53**, 1787–1801.

Hoch, M.P., Fogel, M.L. and Kirchman, D.L. (1992) Isotope fractionation associated with ammonium uptake by a marine bacterium. *Limnol. Oceanogr.* **37**, 1447–1459.

Hodell, D.A., Curtis, J.H., Sierro, F.J. and Raymo, M.E. (2001) Correlation of late Miocene to early Pliocene sequences between the Mediterranean and North Atlantic. *Paleoceanography* **16**, 164–178.

Hodgson, G., Hitchon, B., Taguchi, K., Baker, B. and Peake, E. (1968) Geochemistry of porphyrins, chlorins and polycyclic aromatics in soils, sediments and sedimentary rocks. *Geochim. Cosmochim. Acta* **32**, 737–772.

Hoehler, T.M., Bebout, B.M., and Des Marais, D.J. (2001) The role of microbial mats in the production of reduced gases on the early Earth. *Nature* **412**, 324–327.

Holmes, R., McClelland, J., Sigman, D., Fry, B. and Peterson, B. (1998) Measuring ^{15}N–NH_4^+ in marine, estuarine and fresh waters: An adaptation of the ammonia diffusion method for samples with low ammonium concentrations. *Mar. Chem.* **60**, 235–243.

Holmes, R.M., Aminot, A., Kérouel, R., Hooker, B.A. and Peterson, B.J. (1999) A simple and precise method for measuring ammonium in marine and freshwater ecosystems. *Can. J. Fish. Aquat. Sci.* **56**, 1801–1808.

Honjo, S., Manganini, S.J., Krishfield, R.A. and Francois, R. (2008) Particulate organic carbon fluxes to the ocean interior and factors controlling the biological pump: A synthesis of global sediment trap programs since 1983. *Prog. Oceanogr.* **76**, 217–285.

Hopkinson, B.M., Dupont, C.L., Allen, A.E. and Morel, F.M. (2011) Efficiency of the CO_2-concentrating mechanism of diatoms. *Proc. Natl. Acad. Sci. U.S.A.* **108**, 3830–3837.

Hoyt, P.B. (1966) Chlorophyll-type compounds in soil. *Plant Soil* **25**, 313–328.

Hsü, K., Ryan, W. and Cita, M. (1973) Late Miocene desiccation of the Mediterranean. *Nature* **242**, 240–244.

Hu, X. and Cai, W.J. (2011) An assessment of ocean margin anaerobic processes on oceanic alkalinity budget. *Global Biogeochem. Cycles* **25**, GB3003.

Huang, W.Y. and Meinschein, W. (1979) Sterols as ecological indicators. *Geochim. Cosmochim. Acta* **43**, 739–745.

Iaccarino, S.M., Bertini, A., Di Stefano, A., Ferraro, L., Gennari, R., Grossi, F., Lirer, F., Manzi, V., Menichetti, E. and Ricci Lucchi, M. (2008) The Trave section (Monte dei Corvi, Ancona, Central Italy): an integrated paleontological study of the Messinian deposits. *Stratigraphy* **5**, 281–306.

Imhoff, J.F. (2001) True marine and halophilic anoxygenic phototrophic bacteria. *Arch. Microbiol.* **176**, 243–254.

Isaji, Y., Kawahata, H., Kuroda, J., Yoshimura, T., Ogawa, N.O., Suzuki, A., Shibuya, T., Jiménez-Espejo, F.J., Lugli, S., Santulli, A., Manzi, V., Roveri, M. and Ohkouchi, N. (2017) Biological and physical modification of carbonate system parameters along the salinity gradient in shallow hypersaline solar salterns in Trapani, Italy. *Geochim. Cosmochim. Acta* **208**, 354–367.

Isaji, Y., Kawahata, H., Ohkouchi, N., Murayama, M. and Tamaki, K. (2015a) Terrestrial environmental changes around the Gulf of Aden over the last 210 kyr deduced from the sediment n-alkane record: Implications for the dispersal of Homo sapiens. *Geophys. Res. Lett.* **42**, 1880–1887.

Isaji, Y., Kawahata, H., Ohkouchi, N., Ogawa, N.O., Murayama, M., Inoue, K. and Tamaki, K. (2015b) Varying responses to Indian monsoons during the past 220 kyr recorded in deep-sea sediments in inner and outer regions of the Gulf of Aden. J. Geophys. Res. Oceans **120**, 7253–7270.

Isobe, K., Suwa, Y., Ikutani, J., Kuroiwa, M., Makita, T., Takebayashi, Y., Yoh, M., Otsuka, S., Senoo, K. and Ohmori, M. (2011) Analytical techniques for quantifying

$^{15}N/^{14}N$ of nitrate, nitrite, total dissolved nitrogen and ammonium in environmental samples using a gas chromatograph equipped with a quadrupole mass spectrometer. *Microbes Environ.* **26**, 46–53.

Ivanovic, R.F., Valdes, P.J., Flecker, R., and Gutjahr, M. (2014) Modelling global-scale climate impacts of the late Miocene Messinian Salinity Crisis. *Clim. Past* **10**, 607–622.

Javor, B.J. (1983) Planktonic standing crop and nutrients in a saltern ecosystem. *Limnol. Oceanogr.* **28**, 153–159.

Jeffrey, S., Sielicki, M. and Haxo, F.T. (1975) Chloroplast pigment patterns in dinoflagellates. *J. Phycol.* **11**, 374–384.

Joint, I., Henriksen, P., Garde, K. and Riemann, B. (2002) Primary production, nutrient assimilation and microzooplankton grazing along a hypersaline gradient. *FEMS Microbiol. Ecol.* **39**, 245–257.

Jones, B.F., Eugster, H.P. and Rettig, S.L. (1977) Hydrochemistry of the lake Magadi basin, Kenya. *Geochim. Cosmochim. Acta* **41**, 53–72.

Jørgensen B.B. (1994a) Diffusion processes and boundary layers in microbial mats. In *Microbial Mats: Structure, Development and Environmental Significance* (eds. Stal L.J. and Caumette P.). Springer, Berlin. NATO ASI Series G, Vol. 35, pp. 243–253.

Jørgensen, B.B. (1994b) Sulfate reduction and thiosulfate transformations in a cyanobacterial mat during a diel oxygen cycle. *FEMS Microbiol. Ecol.* **13**, 303–312.

Junium, C.K. and Arthur, M.A. (2007) Nitrogen cycling during the Cretaceous, Cenomanian-Turonian oceanic anoxic event II. *Geochem. Geophys. Geosyst.* **8**.

Junium, C.K., Freeman, K.H. and Arthur, M.A. (2015) Controls on the stratigraphic distribution and nitrogen isotopic composition of zinc, vanadyl and free base porphyrins through Oceanic Anoxic Event 2 at Demerara Rise. *Org. Geochem.* **80**, 60–71.

Kaplan, A., Badger, M.R. and Berry, J.A. (1980) Photosynthesis and the intracellular inorganic carbon pool in the bluegreen alga *Anabaena variabilis*: response to external CO_2 concentration. *Planta* **149**, 219–226.

Karcz, I. and Zak, I. (1987) Bedforms in salt deposits of the Dead sea brines. *J. Sed. Res.* **57**, 723–735.

Karl, D., Letelier, R., Tupas, L. and Dore, J. (1997) The role of nitrogen fixation in biogeochemical cycling in the subtropical North Pacific Ocean. *Nature* **388**, 533–538.

Karl, D.M., Church, M.J., Dore, J.E., Letelier, R.M. and Mahaffey, C. (2012) Predictable and efficient carbon sequestration in the North Pacific Ocean supported by symbiotic nitrogen fixation. *Proc. Natl. Acad. Sci. U.S.A.* **109**, 1842–1849.

Karuso, P., Bergquist, P.R., Buckleton, J.S., Cambie, R.C., Clark, G.R. and Rickard, C.E. (1986) 13^2, 17^3-Cyclopheophorbide enol, the first porphyrin isolated from a sponge.

Tetrahedron Lett. **27**, 2177–2178.

Kashiwabara, T., Oishi, Y., Sakaguchi, A., Sugiyama, T., Usui, A. and Takahashi, Y. (2014) Chemical processes for the extreme enrichment of tellurium into marine ferromanganese oxides. *Geochim. Cosmochim. Acta* **131**, 150–163.

Kashiyama, Y., Kitazato, H. and Ohkouchi, N. (2007) An improved method for isolation and purification of sedimentary porphyrins by high-performance liquid chromatography for compound-specific isotopic analysis. *J. Chromatogr. A* **1138**, 73–83.

Kashiyama, Y., Ogawa, N., Shiro, M., Tada, R., Kitazato, H. and Ohkouchi, N. (2008a) Reconstruction of the biogeochemistry and ecology of photoautotrophs based on the nitrogen and carbon isotopic compositions of vanadyl porphyrins from Miocene siliceous sediments. *Biogeosciences* **5**, 361–409.

Kashiyama, Y., Ogawa, N.O., Kuroda, J., Shiro, M., Nomoto, S., Tada, R., Kitazato, H. and Ohkouchi, N. (2008b) Diazotrophic cyanobacteria as the major photoautotrophs during mid-Cretaceous oceanic anoxic events: Nitrogen and carbon isotopic evidence from sedimentary porphyrin. *Org. Geochem.* **39**, 532–549.

Kashiyama, Y., Ogawa, N.O., Nomoto, S., Kitazato, H. and Ohkouchi, N. (2010) Nitrogen and carbon isotopic compositions of copper, nickel, and vanadyl porphyrins in Cretaceous black shales. In *Earth, Life, and Isotopes* (eds. Ohkouchi N., Tayasu I., and Koba K.). Kyoto University Press, Kyoto. pp. 313–335.

Kashiyama, Y., Yokoyama, A., Kinoshita, Y., Shoji, S., Miyashiya, H., Shiratori, T., Suga, H., Ishikawa, K., Ishikawa, A. and Inouye, I. (2012) Ubiquity and quantitative significance of detoxification catabolism of chlorophyll associated with protistan herbivory. *Proc. Natl. Acad. Sci. U.S.A.* **109**, 17328–17335.

Katase, T. and Wada, E. (1990) Isolation of chlorophyll a in *Microcystis spp.* for determination of stable isotopes of carbon and nitrogen, and variation in Suwa Lake. *Bunseki Kagaku* **39**, 451–456.

Kawahata, H., Suzuki, A. and Ohta, H. (2000) Export fluxes in the western Pacific warm pool. *Deep Sea Res. Part I Oceanogr. Res. Pap.* **47**, 2061–2091.

Keeling, C.D. (1958) The concentration and isotopic abundances of atmospheric carbon dioxide in rural areas. *Geochim. Cosmochim. Acta* **13**, 322–334.

Keely, B., Blake, S., Schaeffer, P. and Maxwell, J. (1995) Distributions of pigments in the organic matter of marls from the Vena del Gesso evaporitic sequence. *Org. Geochem.* **23**, 527–539.

Keely, B., Harris, P., Popp, B., Hayes, J., Meischner, D. and Maxwell, J. (1994) Porphyrin and chlorin distributions in a Late Pliocene lacustrine sediment. *Geochim. Cosmochim. Acta* **58**, 3691–3701.

Keely, B.J. (2006) Geochemistry of chlorophylls, Chlorophylls and Bacteriochlorophylls. Springer, pp. 535–561.

Kemp, A.E., Pearce, R.B., Koizumi, I., Pike, J. and Rance, S.J. (1999) The role of mat-forming diatoms in the formation of Mediterranean sapropels. *Nature* **398**, 57–61.

Kemp, A.E. and Villareal, T.A. (2013) High diatom production and export in stratified waters–A potential negative feedback to global warming. *Prog. Oceanogr.* **119**, 4–23.

Kenig, F., Sinninghe Damsté, J.S., Frewin, N.L., Hayes, J. and De Leeuw, J.W. (1995) Molecular indicators for palaeoenvironmental change in a Messinian evaporitic sequence (Vena del Gesso, Italy). II: High-resolution variations in abundances and ^{13}C contents of free and sulphur-bound carbon skeletons in a single marl bed. *Org. Geochem.* **23**, 485–526.

Knauth, L.P. (1998). Salinity history of the Earth's early ocean. *Nature* **395**, 554–555.

Kohnen, M., Sinninghe Damsté, J.S. and De Leeuw, J.W. (1991) Biases from natural sulphurization in palaeoenvironmental reconstruction based on hydrocarbon biomarker distributions. *Nature* **349**, 775–778.

Kohnen, M.E., Schouten, S., Sinninghe Damsté, J.S., de Leeuw, J.W., Merritt, D.A. and Hayes, J. (1992) Recognition of paleobiochemicals by a combined molecular sulfur and isotope geochemical approach. *Science*, **256**, 358–362.

Koizumi, Y., Kojima, H., Oguri, K., Kitazato, H. and Fukui, M. (2004) Vertical and temporal shifts in microbial communities in the water column and sediment of saline meromictic Lake Kaiike (Japan), as determined by a 16S rDNA-based analysis, and related to physicochemical gradients. *Environ. Microbiol.* **6**, 622–637.

Kouduka, M., Tanabe, A., Yamamoto, S., Yanagawa, K., Nakamura, Y., Akiba, F., Tomaru, H., Toju, H. and Suzuki, Y. (2017) Eukaryotic diversity in late Pleistocene marine sediments around a shallow methane hydrate deposit in the Japan Sea. *Geobiology*, **15**, 715–727.

Kouwenhoven, T., Hilgen, F. and Van der Zwaan, G. (2003) Late Tortonian–early Messinian stepwise disruption of the Mediterranean–Atlantic connections: constraints from benthic foraminiferal and geochemical data. *Palaeogeogr. Palaeoclimatol. Palaeoecol.* **198**, 303–319.

Kouwenhoven, T., Morigi, C., Negri, A., Giunta, S., Krijgsman, W. and Rouchy, J.M. (2006) Paleoenvironmental evolution of the eastern Mediterranean during the Messinian: constraints from integrated microfossil data of the Pissouri Basin (Cyprus). *Mar. Micropaleontol.* **60**, 17–44.

Krijgsman, W., Fortuin, A., Hilgen, F. and Sierro, F. (2001) Astrochronology for the Messinian Sorbas basin (SE Spain) and orbital (precessional) forcing for evaporite cyclicity. *Sediment. Geol.* **140**, 43–60.

Krijgsman, W., Hilgen, F., Raffi, I., Sierro, F. and Wilson, D. (1999) Chronology, causes and progression of the Messinian salinity crisis. *Nature* **400**, 652–655.

Krijgsman, W., Leewis, M.E., Garcés, M., Kouwenhoven, T.J., Kuiper, K.F. and Sierro, F.J. (2006) Tectonic control for evaporite formation in the Eastern Betics (Tortonian; Spain). *Sediment. Geol.* **188**, 155–170.

Krijgsman, W. and Meijer, P.T. (2008) Depositional environments of the Mediterranean "Lower Evaporites" of the Messinian salinity crisis: Constraints from quantitative analyses. *Mar. Geol.* **253**, 73–81.

Kroopnick, P. (1985) The distribution of ^{13}C of ΣCO_2 in the world oceans. *Deep Sea Res. Part I Oceanogr. Res. Pap.* **32**, 57–84.

Krumgalz B. S. (1980) Salt effect on the pH of hypersaline solutions. In: *Hypersaline Brines and Evaporitic Environments. Developments in Sedimentology, vol. 28* (eds, Nissenbaum A.). Elsevier, Amsterdam. pp. 73–83.

Kuroda, J., Jiménez-Espejo, F.J., Nozaki, T., Gennari, R., Lugli, S., Manzi, V., Roveri, M., Flecker, R., Sierro, F.J., Yoshimura, T., Suzuki, K. and Ohkouchi, N. (2016) Miocene to Pleistocene osmium isotopic records of the Mediterranean sediments. *Paleoceanography* **31**, 148–166.

Lazar, B. and Erez, J. (1992) Carbon geochemistry of marine-derived brines: I. ^{13}C depletions due to intense photosynthesis. *Geochim. Cosmochim. Acta* **56**, 335-345.

Lazar, B., Starinsky, A., Katz, A., Sass, E. and Ben-Yaakov, S. (1983) The carbonate system in hypersaline solutions: alkalinity and $CaCO_3$ solubility of evaporated seawater. *Limnol. Oceanogr.* **28**, 978–986.

Ley, R.E., Harris, J.K., Wilcox, J., Spear, J.R., Miller, S.R., Bebout, B.M., Maresca, J.A., Bryant, D.A., Sogin, M.L. and Pace, N.R. (2006) Unexpected diversity and complexity of the Guerrero Negro hypersaline microbial mat. *Appl. Environ. Microbiol.* **72**, 3685–3695.

Li, L., Lollar, B.S., Li, H., Wortmann, U.G. and Lacrampe-Couloume, G. (2012) Ammonium stability and nitrogen isotope fractionations for–NH_3(aq)–NH_3(gas) systems at 20–70°C and pH of 2–13: Applications to habitability and nitrogen cycling in low-temperature hydrothermal systems. *Geochim. Cosmochim. Acta* **84**, 280–296.

Li, Y.H. and Tsui, T.F. (1971) The solubility of CO_2 in water and sea water. *J. Geophys. Res.* **76**, 4203–4207.

Liu, K.K., Kao, S.J., Chiang, K.P., Gong, G.C., Chang, J., Cheng, J.S. and Lan, C.Y. (2013) Concentration dependent nitrogen isotope fractionation during ammonium uptake by phytoplankton under an algal bloom condition in the Danshuei estuary, northern Taiwan. *Mar. Chem.* **157**, 242–252.

Lofi, J., Gorini, C., Berné, S., Clauzon, G., Tadeu Dos Reis, A., Ryan, W.B.F. and Steckler,

M.S. (2005) Erosional processes and paleo-environmental changes in the Western Gulf of Lions (SW France) during the Messinian Salinity Crisis. *Mar. Geol.* **217**, 1–30.

Lofi, J., Sage, F., Déverchère, J., Loncke, L., Maillard, A., Gaullier, V., Thinon, I., Gillet, H., Guennoc, P. and Gorini, C. (2011) Refining our knowledge of the Messinian salinity crisis records in the offshore domain through multi-site seismic analysis. *Bull. Soc. Geol. France* **182**, 163–180.

Logan B. W. (1987) The MacLeod evaporite basin, western Australia. Holocene environments, sediments and geological evolution. *AAPG Memoir* **44**, 1–140.

Louda, J., Neto, R., Magalhaes, A. and Schneider, V. (2008) Pigment alterations in the brown mussel *Perna perna*. *Comp. Biochem. Physiol. B Biochem. Mol. Biol.* **150**, 385–394.

Lowenstein, T.K. and Hardie, L.A. (1985) Criteria for the recognition of salt-pan evaporites. *Sedimentology* **32**, 627–644.

Lowenstein, T.K., Schubert, B.A. and Timofeeff, M.N. (2011) Microbial communities in fluid inclusions and long-term survival in halite. *GSA Today* **21**, 4–9.

Lugli, S., Bassetti, M.A., Manzi, V., Barbieri, M., Longinelli, A. and Roveri, M. (2007) The Messinian 'Vena del Gesso' evaporites revisited: characterization of isotopic composition and organic matter. *Geological Society, London, Special Publications* **285**, 179–190.

Lugli, S., Manzi, V., Roveri, M. and Schreiber B., C. (2010) The Primary Lower Gypsum in the Mediterranean: A new facies interpretation for the first stage of the Messinian salinity crisis. *Palaeogeogr. Palaeoclimatol. Palaeoecol.* **297**, 83–99.

Lugli, S., Schreiber, B.C. and Triberti, B. (1999) Giant polygons in the Realmonte mine (Agrigento, Sicily): evidence for the desiccation of a Messinian halite basin. *J. Sed. Res.* **69**, 764–771.

Mahaffey, C., Michaels, A.F. and Capone, D.G. (2005) The conundrum of marine N_2 fixation. *Am. J. Sci.* **305**, 546–595.

Manzi, V., Gennari, R., Lugli, S., Roveri, M., Scafetta, N. and Schreiber, B.C. (2012) High-frequency cyclicity in the Mediterranean Messinian evaporites: Evidence for solar-lunar climate forcing. *J. Sed. Res.* **82**, 991–1005.

Manzi, V., Lugli, S., Roveri, M. and Charlotte Schreiber, B. (2009) A new facies model for the Upper Gypsum of Sicily (Italy): chronological and palaeoenvironmental constraints for the Messinian salinity crisis in the Mediterranean. *Sedimentology* **56**, 1937–1960.

Manzi, V., Roveri, M., Gennari, R., Bertini, A., Biffi, U., Giunta, S., Iaccarino, S.M., Lanci, L., Lugli, S. and Negri, A. (2007) The deep-water counterpart of the Messinian Lower Evaporites in the Apennine foredeep: the Fanantello section (Northern

Apennines, Italy). *Palaeogeogr. Palaeoclimatol. Palaeoecol.* **251**, 470–499.

Mariotti, A., Germon, J., Hubert, P., Kaiser, P., Letolle, R., Tardieux, A. and Tardieux, P. (1981) Experimental determination of nitrogen kinetic isotope fractionation: some principles; illustration for the denitrification and nitrification processes. *Plant Soil* **62**, 413–430.

Matile, P., Hortensteiner, S., Thomas, H. and Krautler, B. (1996) Chlorophyll breakdown in senescent leaves. *Plant Physiol.* **112**, 1403–1409.

Mawson, D.H. and Keely, B.J. (2008) Novel functionalised chlorins in sediments of the Messinian Vena del Gesso evaporitic sequence: Evidence for a facile route to reduction for biomarkers. *Org. Geochem.* **39**, 203–209.

McCaffrey, M., Lazar, B. and Holland, H. (1987) The evaporation path of seawater and the coprecipitation of Br^- and K^+ with halite. *J. Sed. Res.* **57**, 928–937.

McGenity, T.J., Gemmell, R.T., Grant, W.D. and Stan-Lotter, H. (2000) Origins of halophilic microorganisms in ancient salt deposits. *Environ. Microbiol.* **2**, 243–250.

McGillis, W.R. and Wanninkhof, R. (2006) Aqueous CO_2 gradients for air–sea flux estimates. *Mar. Chem.* **98**, 100–108.

Meijer, P.T. (2012) Hydraulic theory of sea straits applied to the onset of the Messinian Salinity Crisis. *Mar. Geol.* **326**, 131–139.

Meybeck, M. (1982) Carbon, nitrogen, and phosphorus transport by world rivers. *Am. J. Sci.* **282**, 401–450.

Meyers, P.A. and Arnaboldi, M. (2008) Paleoceanographic implications of nitrogen and organic carbon isotopic excursions in mid-Pleistocene sapropels from the Tyrrhenian and Levantine Basins, Mediterranean Sea. *Palaeogeogr. Palaeoclimatol. Palaeoecol.* **266**, 112–118.

Meyers, P.A. and Eadie, B.J. (1993) Sources, degradation and recycling of organic matter associated with sinking particles in Lake Michigan. *Org. Geochem.* **20**, 47–56.

Milder, J.C., Montoya, J.P. and Altabet, M.A. (1999) Carbon and nitrogen stable isotope ratios at sites 969 and 974: Interpreting spatial gradients in sapropel properties, *ODP Scientific Results* **161**, 401–411.

Minagawa, M., Ohashi, M., Kuramoto, T. and Noda, N. (2001) $\delta^{15}N$ of PON and nitrate as a clue to the origin and transformation of nitrogen in the subarctic North Pacific and its marginal sea. *J. Oceanogr.* **57**, 285–300.

Minagawa, M. and Wada, E. (1986) Nitrogen isotope ratios of red tide organisms in the East China Sea: a characterization of biological nitrogen fixation. *Mar. Chem.* **19**, 245–259.

Miyake, Y., and Wada, E. (1967) The abundance ratio of $^{15}N/^{14}N$ in marine environments. *Records of Oceanographic Works in Japan* **9**, 37–53.

Moisander, P.H., Beinart, R.A., Hewson, I., White, A.E., Johnson, K.S., Carlson, C.A., Montoya, J.P. and Zehr, J.P. (2010) Unicellular cyanobacterial distributions broaden the oceanic N_2 fixation domain. *Science* **327**, 1512–1514.

Mook, W., Bommerson, J. and Staverman, W. (1974) Carbon isotope fractionation between dissolved bicarbonate and gaseous carbon dioxide. *Earth. Planet. Sci. Lett.* **22**, 169–176.

Naeher, S., Suga, H., Ogawa, N.O., Schubert, C.J., Grice, K. and Ohkouchi, N. (2016a) Compound-specific carbon and nitrogen isotopic compositions of chlorophyll a and its derivatives reveal the eutrophication history of Lake Zurich (Switzerland). *Chem. Geol.* **443**, 210–219.

Naeher, S., Suga, H., Ogawa, N.O., Takano, Y., Schubert, C.J., Grice, K. and Ohkouchi, N. (2016b) Distributions and compound-specific isotopic signatures of sedimentary chlorins reflect the composition of photoautotrophic communities and their carbon and nitrogen sources in Swiss lakes and the Black Sea. *Chem. Geol.* **443**, 198–209.

Naraoka, H. and Ishiwatari, R. (2000) Molecular and isotopic abundances of long-chain *n*-fatty acids in open marine sediments of the western North Pacific. *Chem. Geol.* **165**, 23–36.

Natalicchio, M., Birgel, D., Peckmann, J., Lozar, F., Carnevale, G., Liu, X., Hinrichs, K.U. and Pierre, F.D. (2017) An archaeal biomarker record of paleoenvironmental change across the onset of the Messinian salinity crisis in the absence of evaporites (Piedmont Basin, Italy). *Org. Geochem.* **113**, 242–253.

Nishizawa, M., Koba, K., Makabe, A., Yoshida, N., Kaneko, M., Hirao, S., Ishibashi, J., Yamanaka, T., Shibuya, T. and Kikuchi, T. (2013) Nitrification-driven forms of nitrogen metabolism in microbial mat communities thriving along an ammonium-enriched subsurface geothermal stream. *Geochim. Cosmochim. Acta* **113**, 152-173.

Nissenbaum, A., Stiller, M. and Nishri A. (1990) Nutrients in pore waters from Dead Sea sediments, *Hydrobiologia*, **197**, 83–89.

O'Brian, M.R. and Thöny-Meyer, L. (2002) Biochemistry, regulation and genomics of haem biosynthesis in prokaryotes. *Adv. Microb. Physiol.* **46**, 257–318.

Ocampo, R., Callot, H., Albrecht, P. and Kintzinger, J. (1984) A novel chlorophyll *c* related petroporphyrin in oil shale. *Tetrahedron Lett.* **25**, 2589–2592.

Ocampo, R., Callot, H., Albrecht, P., Popp, B., Horowitz, M. and Hayes, J. (1989) Different isotope compositions of C_{32} DPEP and C_{32} etioporphyrin III in oil shale. *Naturwissenschaften* **76**, 419–421.

Ogawa, N.O., Nagata, T., Kitazato, H. and Ohkouchi, N. (2010) Ultra-sensitive elemental analyzer/isotope ratio mass spectrometer for stable nitrogen and carbon isotope analyses. In *Earth, Life, and Isotopes* (eds. Ohkouchi N., Tayasu I., and Koba K.).

Kyoto University Press, Kyoto., pp. 339–353.

Ohkouchi, N., Kashiyama, Y., Kuroda, J., Ogawa, N. and Kitazato, H. (2006) The importance of diazotrophic cyanobacteria as primary producers during Cretaceous Oceanic Anoxic Event 2. *Biogeosciences* **3**, 467–478.

Ohkouchi, N., Kawamura, K., Kawahata, H. and Taira, A. (1997) Latitudinal distributions of terrestrial biomarkers in the sediments from the Central Pacific. *Geochim. Cosmochim. Acta* **61**, 1911–1918.

Ohkouchi, N., Nakajima, Y., Ogawa, N.O., Chikaraishi, Y., Suga, H., Sakai, S. and Kitazato, H. (2008) Carbon isotopic composition of the tetrapyrrole nucleus in chloropigments from a saline meromictic lake: A mechanistic view for interpreting the isotopic signature of alkyl porphyrins in geological samples. *Org. Geochem.* **39**, 521–531.

Ohkouchi, N., Nakajima, Y., Okada, H., Ogawa, N.O., Suga, H., Oguri, K. and Kitazato, H. (2005) Biogeochemical processes in the saline meromictic Lake Kaiike, Japan: implications from molecular isotopic evidences of photosynthetic pigments. *Environ. Microbiol.* **7**, 1009–1016.

Ohkouchi, N., Ogawa, N.O., Chikaraishi, Y., Tanaka, H. and Wada, E. (2015) Biochemical and physiological bases for the use of carbon and nitrogen isotopes in environmental and ecological studies. *Prog. Earth Planet. Sci.* **2**, 1.

Ohkouchi, N. and Takano, Y. (2014) Organic nitrogen: sources, fates, and chemistry. In *Treatise on Geochemistry ed.2*, (eds. Holland, H., Turekian, K.) Elsevier, Oxford, vol. 12, pp. 251–289.

Ojha, L., Wilhelm, M.B., Murchie, S.L., McEwen, A.S., Wray, J.J., Hanley, J., Massé, M. and Chojnacki, M. (2015) Spectral evidence for hydrated salts in recurring slope lineae on Mars. *Nat. Geosci.* **8**, 829–832.

Ollivier, B., Caumette, P., Garcia, J.L. and Mah, R. (1994) Anaerobic bacteria from hypersaline environments. *Microbiol. Rev.* **58**, 27–38.

Omodeo Salé, S., Gennari, R., Lugli, S., Manzi, V. and Roveri, M. (2012) Tectonic and climatic control on the Late Messinian sedimentary evolution of the Nijar Basin (Betic Cordillera, Southern Spain). *Basin Research* **24**, 314-337.

Omoregie, E.O., Crumbliss, L.L., Bebout, B.M. and Zehr, J.P. (2004) Comparison of diazotroph community structure in Lyngbya sp. and Microcoleus chthonoplastes dominated microbial mats from Guerrero Negro, Baja, Mexico. *FEMS Microbiol. Ecol.* **47**, 305–308.

Oren, A. (1999) Bioenergetic aspects of halophilism. *Microbiol. Mol. Biol. Rev.* **63**, 334–348.

Oren, A. (2002) Diversity of halophilic microorganisms: environments, phylogeny,

physiology, and applications. *J. Ind. Microbiol. Biotechnol.* **28**, 56–63.

Oren, A. (2005) A hundred years of *Dunaliella* research: 1905–2005. *Saline systems* **1**, 2.

Oren, A. (2009) Saltern evaporation ponds as model systems for the study of primary production processes under hypersaline conditions. *Aquat. Microb. Ecol.* **56**, 193–204.

Oren, A. (2010) The dying Dead Sea: the microbiology of an increasingly extreme environment. *Lakes & Reservoirs: Research & Management* **15**, 215–222.

Oro, J., Laseter, J. and Weber, D. (1966) Alkanes in fungal spores. *Science* **154**, 399-400.

Orphan, V., Jahnke, L., Embaye, T., Turk, K., Pernthaler, A., Summons, R. and Des Marais, D. (2008) Characterization and spatial distribution of methanogens and methanogenic biosignatures in hypersaline microbial mats of Baja California. *Geobiology* **6**, 376–393.

Orszag-Sperber, F. (2006) Changing perspectives in the concept of "Lago-Mare" in Mediterranean Late Miocene evolution. *Sediment. Geol.* **188**, 259–277.

Ourisson, G. and Albrecht, P. (1992) Hopanoids. 1. Geohopanoids: the most abundant natural products on Earth? *Acc. Chem. Res.* **25**, 398–402.

Pagani, M., Freeman, K.H. and Arthur, M.A. (1999) Late Miocene atmospheric CO_2 concentrations and the expansion of C4 grasses. *Science* **285**, 876–879.

Pancost, R.D., Freeman, K.H., Wakeham, S.G. and Robertson, C.Y. (1997) Controls on carbon isotope fractionation by diatoms in the Peru upwelling region. *Geochim. Cosmochim. Acta* **61**, 4983–4991.

Panieri, G., Lugli, S., Manzi, V., Roveri, M., Schreiber, B.C. and Palinska, K.A. (2010) Ribosomal RNA gene fragments from fossilized cyanobacteria identified in primary gypsum from the late Miocene, Italy. *Geobiology* **8**, 101–111.

Pantoja, S., Repeta, D.J., Sachs, J.P. and Sigman, D.M. (2002) Stable isotope constraints on the nitrogen cycle of the Mediterranean Sea water column. *Deep Sea Res. Part I Oceanogr. Res. Pap.* **49**, 1609–1621.

Pedrós-Alió, C., Calderón-Paz, J.I., MacLean, M.H., Medina, G., Marrasé, C., Gasol, J.M. and Guixa-Boixereu, N. (2000) The microbial food web along salinity gradients. *FEMS Microbiol. Ecol.* **32**, 143–155.

Pennock, J.R., Velinsky, D.J., Ludlam, J.M., Sharp, J.H. and Fogel, M.L. (1996) Isotopic fractionation of ammonium and nitrate during uptake by *Skeletonema costatum*: Implications for $\delta^{15}N$ dynamics under bloom conditions. *Limnol. Oceanogr.* **41**, 451–459.

Pinckney, J., Paerl, H. and Bebout, B. (1995) Salinity control of benthic microbial mat community production in a Bahamian hypersaline lagoon. *J. Exp. Mar. Bio. Ecol.* **187**, 223–237.

Pinckney, J.L. and Paerl, H.W. (1997) Anoxygenic photosynthesis and nitrogen fixation

by a microbial mat community in a bahamian hypersaline lagoon. *Appl. Environ. Microbiol.* **63**, 420–426.

Popp, B.N., Laws, E.A., Bidigare, R.R., Dore, J.E., Hanson, K.L. and Wakeham, S.G. (1998) Effect of phytoplankton cell geometry on carbon isotopic fractionation. *Geochim. Cosmochim. Acta* **62**, 69–77.

Popp, B.N., Takigiku, R., Hayes, J., Louda, J.W. and Baker, E.W. (1989) The post-Paleozoic chronology and mechanism of ^{13}C depletion in primary marine organic matter. *Am. J. Sci.* **289**, 436–454.

Post, F.J. (1977) The microbial ecology of the Great Salt Lake. *Microb. Ecol.* **3**, 143-165.

Pound, M.J., Haywood, A.M., Salzmann, U. and Riding, J.B. (2012) Global vegetation dynamics and latitudinal temperature gradients during the Mid to Late Miocene (15.97–5.33 Ma). *Earth Sci. Rev.* **112**, 1–22.

Prins, H. and Elzenga, J. (1989) Bicarbonate utilization: function and mechanism. *Aquat. Bot.* **34**, 59–83.

Prowse, W., Chicarelli, M., Keely, B., Kaur, S. and Maxwell, J. (1987) Characterisation of fossil porphyrins of the "di-DPEP" type. *Geochim. Cosmochim. Acta* **51**, 2875–2877.

Pytkowicz, R. (1975) Activity coefficients of bicarbonates and carbonates in seawater. *Limnol. Oceanogr.* **20**, 971–975.

Raven, J. (1997) Inorganic carbon acquisition by marine autotrophs. *Adv. Bot. Res.* **27**, 85–209.

Raven, J.A. (1991) Implications of inorganic carbon utilization: ecology, evolution, and geochemistry. *Can. J. Bot.* **69**, 908–924.

Řeháková, K., Zapomělová, E., Prášil, O., Veselá, J., Medová, H. and Oren, A. (2009) Composition changes of phototrophic microbial communities along the salinity gradient in the solar saltern evaporation ponds of Eilat, Israel. *Hydrobiologia* **636**, 77–88.

Ren, H., Sigman, D.M., Martínez-García, A., Anderson, R.F., Chen, M.T., Ravelo, A.C., Straub, M., Wong, G.T. and Haug, G.H. (2017) Impact of glacial/interglacial sea level change on the ocean nitrogen cycle. *Proc. Natl. Acad. Sci. U.S.A.* **114**, 6759–6766.

Revsbech, N.P., Jorgensen, B.B., Blackburn, T.H. and Cohen, Y. (1983) Microelectrode studies of the photosynthesis and O_2, H_2S, and *p*H profiles of a microbial mat. *Limnol. Oceanogr.* **28**, 1062–1074.

Rigaudier, T., Lécuyer, C., Gardien, V., Suc, J.P. and Martineau, F. (2011) The record of temperature, wind velocity and air humidity in the δD and $\delta^{18}O$ of water inclusions in synthetic and Messinian halites. *Geochim. Cosmochim. Acta* **75**, 4637–4652.

Risatti, J., Rowland, S., Yon, D. and Maxwell, J. (1984) Stereochemical studies of acyclic isoprenoids—XII. Lipids of methanogenic bacteria and possible contributions to

sediments. *Org. Geochem.* **6**, 93–104.

Rohling, E.J., Marino, G. and Grant, K.M. (2015) Mediterranean climate and oceanography, and the periodic development of anoxic events (sapropels). *Earth Sci. Rev.* **143**, 62–97.

Rohmer, M., Bouvier-Nave, P. and Ourisson, G. (1984) Distribution of hopanoid triterpenes in prokaryotes. *Microbiology* **130**, 1137–1150.

Romanek, C.S., Grossman, E.L. and Morse, J.W. (1992) Carbon isotopic fractionation in synthetic aragonite and calcite: effects of temperature and precipitation rate. *Geochim. Cosmochim. Acta* **56**, 419–430.

Rouchy, J.M. and Monty C.L.V. (1981) Stromatolites and cryptalgal laminites associated with Messinian gypsum of Cyprus. In *Phanerozoic Stromatolites*. (eds. Monty, C.L.V.) Springer, Verlag, pp. 155–178.

Rouchy, J.M. and Caruso, A. (2006) The Messinian salinity crisis in the Mediterranean basin: A reassessment of the data and an integrated scenario. *Sediment. Geol.* **188-189**, 35–67.

Roveri, M., Bassetti, M. and Lucchi, F.R. (2001) The Mediterranean Messinian salinity crisis: an Apennine foredeep perspective. *Sediment. Geol.* 140, 201–214.

Roveri, M., Flecker, R., Krijgsman, W., Lofi, J., Lugli, S., Manzi, V., Sierro, F.J., Bertini, A., Camerlenghi, A., De Lange, G., Govers, R., Hilgen, F.J., Hübscher, C., Meijer, P.T. and Stoica, M. (2014) The Messinian Salinity Crisis: Past and future of a great challenge for marine sciences. *Mar. Geol.* **352**, 25–58.

Roveri, M., Gennari, R., Lugli, S. and Manzi, V. (2009) The Terminal Carbonate Complex: the record of sea-level changes during the Messinian salinity crisis. *Geoacta* **8**, e77.

Roveri, M., Lugli, S., Manzi, V. and Schreiber, B.C. (2008) The Messinian Sicilian stratigraphy revisited: new insights for the Messinian salinity crisis. *Terra Nova* **20**, 483–488.

Rueter, J.G. (1988) Iron stimulation of photosynthesis and nitrogen fixation in *Anabaena* 7120 and *Trichodesmium* (Cyanophyceae). *J. Phycol.* **24**, 249–254.

Ryan, W.B. (2009) Decoding the Mediterranean salinity crisis. *Sedimentology* **56**, 95–136.

Sachs, J.P. and Repeta, D.J. (1999) Oligotrophy and nitrogen fixation during eastern Mediterranean sapropel events. *Science* **286**, 2485–2488.

Sachs, J.P., Repeta, D.J. and Goericke, R. (1999) Nitrogen and carbon isotopic ratios of chlorophyll from marine phytoplankton. *Geochim. Cosmochim. Acta* **63**, 1431–1441.

Saino, T. and Hattori, A. (1987) Geographical variation of the water column distrubution of suspended particulate organic nitrogen and its ^{15}N natural abundance in the Pacific and its marginal seas. *Deep Sea Res. Part I Oceanogr. Res. Pap.* **34**, 807–827.

Sakata, K., Yamamoto, K.i., Ishikawa, H., Yagi, A., Etoh, H. and Ina, K. (1990) Chlorophyllone-*a*, a new pheophorbide-a related compound isolated from *Ruditapes philippinarum* as an antioxidative compound. *Tetrahedron Lett.* **31**, 1165–1168.

Saito, T., Shibuya, T., Komiya, T., Kitajima, K., Yamamoto, S., Nishizawa, M., Ueno, Y., Kurosawa, M. and Maruyama, S. (2016) PIXE and microthermometric analyses of fluid inclusions in hydrothermal quartz from the 2.2 Ga Ongeluk Formation, South Africa: Implications for ancient seawater salinity. *Precambr. Res*. **286**, 337–351.

Sanger, J.E. (1988) Fossil pigments in paleoecology and paleolimnology. *Palaeogeogr. Palaeoclimatol. Palaeoecol.* **62**, 343–359.

Sass, E. and Ben-Yaakov, S. (1977) The carbonate system in hypersaline solutions: Dead Sea brines. *Mar. Chem.* **5**, 183–199.

Scalan, R.N. (1958) The isotopic composition, concentration, and chemical state of the nitrogen in igneous rocks. Univ. Arkansas.

Schaeffer, P., Harrison, W., Keely, B. and Maxwell, J. (1995) Product distributions from chemical degradation of kerogens from a marl from a Miocene evaporitic sequence (Vena del Gesso, N. Italy). *Org. Geochem.* **23**, 541–554.

Schaeffer, P., Ocampo, R., Callot, H. and Albrecht, P. (1993) Extraction of bound porphyrins from sulphur-rich sediments and their use for reconstruction of palaeoenvironments. *Nature* **364**, 133–136.

Schaeffer, P., Ocampo, R., Callot, H.J. and Albrecht, P. (1994) Structure determination by deuterium labelling of a sulfur-bound petroporphyrin. *Geochim. Cosmochim. Acta* **58**, 4247-4252.

Scharek, R., Tupas, L.M. and Karl, D.M. (1999) Diatom fluxes to the deep sea in the oligotrophic North Pacific gyre at Station ALOHA. *Mar. Ecol. Prog. Ser.* **182**, 55–67.

Schouten, S., Hartgers, W.A., Lòpez, J.F., Grimalt, J.O. and Damsté, J.S.S. (2001) A molecular isotopic study of ^{13}C-enriched organic matter in evaporitic deposits: recognition of CO_2-limited ecosystems. *Org. Geochem.* **32**, 277–286.

Schouten, S., Pavlović, D., Sinninghe Damsté, J.S. and de Leeuw, J.W. (1993) Nickel boride: an improved desulphurizing agent for sulphur-rich geomacromolecules in polar and asphaltene fractions. *Org. Geochem.* **20**, 901–909.

Schulte, P., Van Geldern, R., Freitag, H., Karim, A., Négrel, P., Petelet-Giraud, E., Probst, A., Probst, J.-L., Telmer, K. and Veizer, J. (2011) Applications of stable water and carbon isotopes in watershed research: Weathering, carbon cycling, and water balances. *Earth Sci. Rev.* **109**, 20–31.

Shackleton, N., Hall, M. and Pate, D. (1995) Pliocene stable isotope stratigraphy of Site 846, *Proc. Ocean Drill. Program Sci. Results* **138**, 337–355.

Shackleton, N.J. (1975) Paleotemperature history of the Cenozoic and the initiation of

Antarctic glaciation: oxygen and carbon isotope analyses in DSDP Sites 277, 279, and 281. *Initial reports of the DSDP* **29**, 743–755.

Shackleton, N.J. (2000) The 100,000-year ice-age cycle identified and found to lag temperature, carbon dioxide, and orbital eccentricity. *Science* **289**, 1897–1902.

Shen, J., Yuan, L., Zhang, J., Li, H., Bai, Z., Chen, X., Zhang, W. and Zhang, F. (2011) Phosphorus dynamics: from soil to plant. *Plant Physiol.* **156**, 997-1005.

Sierro, F., Flores, J., Francés, G., Vazquez, A., Utrilla, R., Zamarreño, I., Erlenkeuser, H. and Barcena, M. (2003) Orbitally-controlled oscillations in planktic communities and cyclic changes in western Mediterranean hydrography during the Messinian. *Palaeogeogr. Palaeoclimatol. Palaeoecol.* **190**, 289–316.

Sierro, F., Flores, J., Zamarreno, I., Vazquez, A., Utrilla, R., Francés, G., Hilgen, F. and Krijgsman, W. (1999) Messinian pre-evaporite sapropels and precession-induced oscillations in western Mediterranean climate. *Mar. Geol.* **153**, 137–146.

Sigman, D., Karsh, K. and Casciotti, K. (2009) Ocean process tracers: nitrogen isotopes in the ocean. In *Encyclopedia of Ocean Sciences* (eds. Steele, J.H., Thorpe, S. and Turekian, K.) Academic Press, New York, pp. 40–54.

Sigman, D.M., Casciotti, K.L., Andreani, M., Barford, C., Galanter, M. and Böhlke, J. (2001) A bacterial method for the nitrogen isotopic analysis of nitrate in seawater and freshwater. *Anal. Chem.* **73**, 4145–4153.

Simon, D., Marzocchi, A., Flecker, R., Lunt, D.J., Hilgen, F.J. and Meijer, P.T. (2017) Quantifying the Mediterranean freshwater budget throughout the late Miocene: New implications for sapropel formation and the Messinian Salinity Crisis. *Earth. Planet. Sci. Lett.* **472**, 25–37.

Simon, D. and Meijer, P.T. (2017) Salinity stratification of the Mediterranean Sea during the Messinian crisis: A first model analysis. *Earth. Planet. Sci. Lett.* **479**, 366–376.

Sinninghe Damsté, J.S. and De Leeuw, J.W. (1990) Analysis, structure and geochemical significance of organically-bound sulphur in the geosphere: state of the art and future research. *Org. Geochem.* **16**, 1077–1101.

Sinninghe Damsté, J.S., Frewin, N.L., Kenig, F. and De Leeuw, J.W. (1995a) Molecular indicators for palaeoenvironmental change in a Messinian evaporitic sequence (Vena del Gesso, Italy). I: Variations in extractable organic matter of ten cyclically deposited marl beds. *Org. Geochem.* **23**, 471–483.

Sinninghe Damsté, J.S., Kenig, F., Koopmans, M.P., Köster, J., Schouten, S., Hayes, J. and de Leeuw, J.W. (1995b) Evidence for gammacerane as an indicator of water column stratification. *Geochim. Cosmochim. Acta* **59**, 1895–1900.

Solorzano, L. (1969) Determination of ammonia in natural waters by the phenolhypochlorite method. *Limnol. Oceanogr.* **14**, 799–801.

Sørensen, K.B., Canfield, D.E. and Oren, A. (2004) Salinity responses of benthic microbial communities in a solar saltern (Eilat, Israel). *Appl. Environ. Microbiol.* **70**, 1608–1616.

Spiro, C., Wong, J., Lytle, F., Greegor, R., Maylotte, D. and Lamson, S. (1984) X-ray absorption spectroscopic investigation of sulfur sites in coal: Organic sulfur identification. *Science* **226**, 48–50.

Stark, J.M. and Hart, S.C. (1996) Diffusion technique for preparing salt solutions, Kjeldahl digests, and persulfate digests for nitrogen-15 analysis. *Soil Sci. Soc. Am. J.* **60**, 1846–1855.

Stauber, J.L. and Jeffrey, S. (1988) Photosynthetic pigments in fifty-one species of marine diatoms. *J. Phycol.* **24**, 158–172.

Stewart, F. H. (1963) Marine evaporites. In *Data of Geochemistry, sixth ed*. USGS professional paper 440-Y.

Stiller, M., Rounick, J. and Shasha, S. (1985) Extreme carbon-isotope enrichments in evaporating brines. *Nature* **316**, 434–435.

Summons, R.E., Bradley, A.S., Jahnke, L.L. and Waldbauer, J.R. (2006) Steroids, triterpenoids and molecular oxygen. *Philos. Trans. R. Soc. Lond. B Biol Sci.* **361**, 951–968.

Summons, R.E., Volkman, J.K. and Boreham, C.J. (1987) Dinosterane and other steroidal hydrocarbons of dinoflagellate origin in sediments and petroleum. *Geochim. Cosmochim. Acta* **51**, 3075–3082.

Sun, X. and Wang, P. (2005) How old is the Asian monsoon system?—Palaeobotanical records from China. *Palaeogeogr. Palaeoclimatol. Palaeoecol.* **222**, 181–222.

Sundararaman, P. and Boreham, C.J. (1993) Comparison of nickel and vanadyl porphyrin distributions of sediments. *Geochim. Cosmochim. Acta* **57**, 1367–1377.

Sutka, R., Ostrom, N., Ostrom, P. and Phanikumar, M. (2004) Stable nitrogen isotope dynamics of dissolved nitrate in a transect from the North Pacific Subtropical Gyre to the Eastern Tropical North Pacific. *Geochim. Cosmochim. Acta* **68**, 517–527.

Sutton, S.R., Bertsch, P.M., Newville, M., Rivers, M., Lanzirotti, A. and Eng, P. (2002) Microfluorescence and microtomography analyses of heterogeneous earth and environmental materials. *Rev. Mineral. Geochem.* **49**, 429–483.

Takishita, K., Chikaraishi, Y., Leger, M.M., Kim, E., Yabuki, A., Ohkouchi, N. and Roger, A.J. (2012) Lateral transfer of tetrahymanol-synthesizing genes has allowed multiple diverse eukaryote lineages to independently adapt to environments without oxygen. *Biol. Direct* **7**, 5.

Tamenori, Y., Morita, M. and Nakamura, T. (2011) Two-dimensional approach to fluorescence yield XANES measurement using a silicon drift detector. *J. Synchrotron*

Rad. **18**, 747–752.

Tamenori, Y., Yoshimura, T., Luan, N.T., Hasegawa, H., Suzuki, A., Kawahata, H. and Iwasaki, N. (2014) Identification of the chemical form of sulfur compounds in the Japanese pink coral (*Corallium elatius*) skeleton using μ-XRF/XAS speciation mapping. *J. Struct. Biol.* **186**, 214–223.

Teske, A., Ramsing, N.B., Habicht, K., Fukui, M., Küver, J., Jørgensen, B.B. and Cohen, Y. (1998) Sulfate-reducing bacteria and their activities in cyanobacterial mats of Solar Lake (Sinai, Egypt). *Appl. Environ. Microbiol.* **64**, 2943–2951.

Thomas, H., Schiettecatte, L., Suykens, K., M Kone, Y., Shadwick, E., F Prowe, A., Bozec, Y., W de Baar, H. and Borges, A. (2009) Enhanced ocean carbon storage from anaerobic alkalinity generation in coastal sediments. *Biogeosciences* **6**, 267–274.

Timofeeff, M., Lowenstein, T., Brennan, S., Demicco, R., Zimmermann, H., Horita, J. and Von Borstel, L. (2001) Evaluating seawater chemistry from fluid inclusions in halite: Examples from modern marine and nonmarine environments. *Geochim. Cosmochim. Acta* **65**, 2293–2300.

Treibs, A. (1936) Chlorophyll and hemin derivatives in organic materials. *Angew. Chem.* **49**, 682–686.

Urey, H.C. (1947) The thermodynamic properties of isotopic substances. *J. Chem. Soc.* **1947**, 562–581.

Vai, G.B. and Ricci Lucchi, F. (1977) Algal crusts, autochthonous and clastic gypsum in a cannibalistic evaporite basin: a case history from the Messinian of Northern Apennines. *Sedimentology* **24**, 211–244.

Valdivieso-Ojeda, J.A., Huerta-Diaz, M.A. and Delgadillo-Hinojosa, F. (2014) High enrichment of molybdenum in hypersaline microbial mats of Guerrero Negro, Baja California Sur, Mexico. *Chem. Geol.* **363**, 341–354.

Van der Laan, E., Gaboardi, S., Hilgen, F. and Lourens, L. (2005) Regional climate and glacial control on high-resolution oxygen isotope records from Ain el Beida (latest Miocene, northwest Morocco): A cyclostratigraphic analysis in the depth and time domain. *Paleoceanography* **20**, PA1001.

Van Gemerden, H. (1993) Microbial mats: a joint venture. *Mar. Geol.* **113**, 3–25.

Van Gemerden, H. and Mas, J. (1995) Ecology of Phototrophic Sulfur Bacteria. In *Anoxygenic Photosynthetic Bacteria. Advances in Photosynthesis and Respiration, vol 2.* (eds. Blankenship, R.E., Madigan, M.T. and Bauer C.E.) Springer, Dordrecht, pp. 49–85.

Velinsky, D.J., Fogel, M.L., Todd, J.F. and Tebo, B.M. (1991) Isotopic fractionation of dissolved ammonium at the oxygen-hydrogen sulfide interface in anoxic waters. *Geophys. Res. Lett.* **18**, 649–652.

Venrick, E. (1974) The distribution and significance of Richelia intracellularis Schmidt in the North Pacific Central Gyre. *Limnol. Oceanogr.* **19**, 437–445.

Verne-Mismer, J., Ocampo, R., Callot, H. and Albrecht, P. (1988) Molecular fossils of chlorophyll *c* of the 17-nor-DPEP series. Structure determination, synthesis, geochemical significance. *Tetrahedron Lett.* **29**, 371–374.

Villareal, T.A., Woods, S., Moore, J.K. and CulverRymsza, K. (1996) Vertical migration of Rhizosolenia mats and their significance to NO_3^- fluxes in the central North Pacific gyre. *J. Plankton Res*. **18**, 1103–1121.

Vo, J., Inwood, W., Hayes, J.M. and Kustu, S. (2013) Mechanism for nitrogen isotope fractionation during ammonium assimilation by *Escherichia coli* K12. *Proc. Natl. Acad. Sci. U.S.A.* **110**, 8696–8701.

Volkman, J.K. (2005) Sterols and other triterpenoids: source specificity and evolution of biosynthetic pathways. *Org. Geochem.* **36**, 139–159.

Volkman, J.K., Allen, D.I., Stevenson, P.L. and Burton, H. (1986) Bacterial and algal hydrocarbons in sediments from a saline Antarctic lake, Ace Lake. *Org. Geochem.* **10**, 671–681.

Volkman, J.K., Barrett, S.M., Blackburn, S.I., Mansour, M.P., Sikes, E.L. and Gelin, F. (1998) Microalgal biomarkers: a review of recent research developments. *Org. Geochem.* **29**, 1163–1179.

Voss, M., Dippner, J.W. and Montoya, J.P. (2001) Nitrogen isotope patterns in the oxygen-deficient waters of the Eastern Tropical North Pacific Ocean. *Deep Sea Res. Part I Oceanogr. Res. Pap.* **48**, 1905–1921.

Wada, E. (1980) Nitrogen isotope fractionation and its significance in biogeochemical processes occurring in marine environments. *Isotope marine chemistry*, 375–398.

Wada, E., Ohki, K., Yoshikawa, S., Parker, P.L., Van Baalen, C., Matsumoto, G.I., Aita, M.N. and Saino, T. (2012) Ecological aspects of carbon and nitrogen isotope ratios of cyanobacteria. *Plankton Benthos Res.* **7**, 135–145.

Ward, B.B. (2008) Nitrification in marine systems. In *Nitrogen in the marine environment*. (eds. Capone, D.G., Bronk, D.A., Mulholland, M.R., and Carpenter, E.J.) Academic Press, New York, pp. 199–261.

Ware, J.R., Smith, S.V. and Reaka-Kudla, M.L. (1992) Coral reefs: sources or sinks of atmospheric CO_2? *Coral Reefs* **11**, 127–130.

Warren, J.K. (2010) Evaporites through time: Tectonic, climatic and eustatic controls in marine and nonmarine deposits. *Earth Sci. Rev.* **98**, 217–268.

Warren, J.K. (2016) *Evaporites: A geological compendium.* Springer, New York, pp. 1813.

Waser, N.A., Yin, K., Yu, Z., Tada, K., Harrison, P.J., Turpin, D.H. and Calvert, S.E. (1998) Nitrogen isotope fractionation during nitrate, ammonium and urea uptake by

marine diatoms and coccolithophores under various conditions of N availability. *Mar. Ecol. Prog. Ser.* **169**, 29–41.

Werne, J.P., Hollander, D.J., Lyons, T.W. and Damsté, J.S.S. (2004) Organic sulfur biogeochemistry: recent advances and future research directions. *Geol. Soc. Spec. Pap.* **379**, 135–150.

Wieland, A., de Beer, D., Damgaard, L.R., Kühl, M., van Dusschoten, D. and Van As, H. (2001) Fine-scale measurement of diffusivity in a microbial mat with nuclear magnetic resonance imaging. *Limnol. Oceanogr.* **46**, 248–259.

Wieland, A. and Kühl, M. (2005) Regulation of photosynthesis and oxygen consumption in a hypersaline cyanobacterial mat (Camargue, France) by irradiance, temperature and salinity. *FEMS Microbiol. Ecol.* **55**, 195–210.

Wieland, A., Zopfi, J., Benthien, M. and Kühl, M. (2005) Biogeochemistry of an iron-rich hypersaline microbial mat (Camargue, France). *Microb. Ecol.* **49**, 34–49.

Wilson, C., Villareal, T.A., Maximenko, N., Bograd, S.J., Montoya, J.P. and Schoenbaechler, C.A. (2008) Biological and physical forcings of late summer chlorophyll blooms at 30N in the oligotrophic Pacific. *J. Mar. Syst.* **69**, 164–176.

Wörmer, L., Elvert, M., Fuchser, J., Lipp, J.S., Buttigieg, P.L., Zabel, M. and Hinrichs, K.U. (2014) Ultra-high-resolution paleoenvironmental records via direct laser-based analysis of lipid biomarkers in sediment core samples. *Proc. Natl. Acad. Sci. U.S.A.* **111**, 15669–15674.

Yannarell, A.C. and Paerl, H.W. (2007) Effects of salinity and light on organic carbon and nitrogen uptake in a hypersaline microbial mat. *FEMS Microbiol. Ecol.* **62**, 345-353.

Yool, A., Martin, A.P., Fernández, C. and Clark, D.R. (2007) The significance of nitrification for oceanic new production. *Nature* **447**, 999–1002.

York, J.K., Tomasky, G., Valiela, I. and Repeta, D.J. (2007) Stable isotopic detection of ammonium and nitrate assimilation by phytoplankton in the Waquoit Bay estuarine system. *Limnol. Oceanogr.* **52**, 144–155.

Yoshimura, T., Kuroda, J., Lugli, S., Tamenori, Y., Ogawa, N.O., Jiménez-Espejo, F.J., Isaji, Y., Roveri, M., Manzi, V., Kawahata, H. and Ohkouchi, N. (2016) An X-ray spectroscopic perspective on Messinian evaporite from Sicily: Sedimentary fabrics, element distributions, and chemical environments of S and Mg. *Geochem. Geophys. Geosyst.* **17**, 1383–1400.

Yoshimura, T., Tamenori, Y., Iwasaki, N., Hasegawa, H., Suzuki, A. and Kawahata, H. (2013) Magnesium K-edge XANES spectroscopy of geological standards. *J. Synchrotron Rad.* **20**, 734–740.

Yoshimura, T., Tamenori, Y., Takahashi, O., Nguyen, L.T., Hasegawa, H., Iwasaki, N., Kuroyanagi, A., Suzuki, A. and Kawahata, H. (2015) Mg coordination in biogenic

carbonates constrained by theoretical and experimental XANES. *Earth. Planet. Sci. Lett.* **421**, 68–74.

Zachos, J., Pagani, M., Sloan, L., Thomas, E. and Billups, K. (2001) Trends, rhythms, and aberrations in global climate 65 Ma to present. *Science* **292**, 686–693.

Zachos, J.C., Dickens, G.R. and Zeebe, R.E. (2008) An early Cenozoic perspective on greenhouse warming and carbon-cycle dynamics. *Nature* **451**, 279–283.

Zehr, J.P. and Ward, B.B. (2002) Nitrogen cycling in the ocean: new perspectives on processes and paradigms. *Appl. Environ. Microbiol.* **68**, 1015–1024.

Zhang, X., Sigman, D.M., Morel, F.M. and Kraepiel, A.M. (2014) Nitrogen isotope fractionation by alternative nitrogenases and past ocean anoxia. *Proc. Natl. Acad. Sci. U.S.A.* **111**, 4782–4787.

Zhisheng, A., Kutzbach, J.E., Prell, W.L. and Porter, S.C. (2001) Evolution of Asian monsoons and phased uplift of the Himalaya–Tibetan plateau since Late Miocene times. *Nature* **411**, 62–66.